EFFECTS OF RF POWER AND TUBE WALL TEMPERATURE ON PLASMA STABILITY AND ANALYTE EMISSION IN FURNACE ATOMIZATION PLASMA EXCITATION SPECTROMETRY

by

MD. MAHBUBUR RAHMAN
B. Sc. , University of Dhaka, Bangladesh, 1986

A DISSERTATION SUBMITTED IN PARTIAL FULFILLMENT OF THE REQUIREMENT FOR THE DEGREE OF MASTER OF SCIENCE IN THE FACULTY OF GRADUATE STUDIES DEPARTMENT OF CHEMISTRY

We accept this dissertation as conforming
to the required standard

THE UNIVERSITY OF BRITISH COLUMBIA
AUGUST 1994

In presenting this thesis in partial fulfillment of the requirements for an advanced degree at the University of British Columbia, I agree that the Library shall make it freely available for reference and study. I further agree that permission for extensive copying of this thesis for scholarly purposes may be granted by the head of my department or by his or her representatives. It is understood that copying or publication of this thesis for financial gain shall not be allowed without my written permission.

(Signature)

Department of Chemistry

The University of British Columbia
Vancouver, Canada

Date 09. 09. 1996

ABSTRACT

Furnace Atomization Plasma Excitation Spectrometry (FAPES) is a relatively new emission spectrochemical method. For analyte atomization and excitation, this method employs a graphite furnace and an atmospheric pressure plasma sustained inside the furnace. The main objective of this work was to characterize the plasma at high rf powers, up to 150 W, during the analyte atomization cycle.

The temporal response of CO^+ and He (I) line at different rf powers shows complex emission characteristics during the atomization step. The intensity of CO^+ and He (I) emission decreases suddenly at higher furnace temperature and higher rf powers. This sudden decrease of intensity indicates the extinguishing of plasma at higher temperature as a result of the changing in power coupling efficiency between the load impedance and output impedance of the rf oscillator. The reflected power level also increases with increasing forward power and does not depend absolutely on the furnace wall temperature but on the temperature of rf center electrode.

The spatial distribution of analyte in the plasma shows an increase in emission intensity from the center of the furnace toward the wall, reaches a maximum at 1.25 mm from the center, followed by a decrease. Both atomic absorption and emission experiments show a non - uniform temperature distribution along the length of the rf electrode. In comparison to the furnace wall , the temperature lag of the rf electrode causes analyte condensation on

the rf electrode and subsequent re-vaporization, resulting in two peaks in the temporal response of the analyte. Analyte condensation on the rf electrode is severe at lower rf powers but at higher rf powers, for example 125 W, the rf electrode becomes too hot to act as a second surface and, as a result, a single peak is observed.

The effect of rf power on analyte signal is a decrease in integrated intensity for both emission and absorption at rf powers higher than 30 W due to several reasons including pre-atomization loss of analyte, a change in excitation characteristics, and an increase in ionization of analyte at higher rf powers. Furthermore, the shape of the peaks shows that the residence time for excited Ag atoms is shorter than that for ground state atoms at rf power 50 W and more. This observation suggests that some of the ground state atoms do not become excited due to quenching of the plasma which is likely because of the change in power coupling efficiency between the load impedance and output impedance due to rapid change of temperature and / or rapid change in thermionic electron density in the furnace.

TABLE OF CONTENTS

LIST OF FIGURES

FIGURES **PAGE**

LIST OF ABBREVIATIONS

AAS	atomic absorption spectrometry
a. c.	alternating current
ADC	analog - to - digital converter
AES	atomic emission spectrometry
APF-CCP	atmospheric pressure furnace capacitively coupled plasma
CFAES	carbon furnace atomic emission spectrometry
CMP	capacitive microwave plasma
CRA	carbon rod atomizer
d. c.	direct current
EIE	easily ionizable element
ETAAS	electrothermal atomic absorption spectrometry
FAPES	furnace atomization plasma excitation spectrometry
FANES	furnace atomization non-thermal excitation spectrometry
FWHM	full - width of half maximum
GD	glow discharge
GF	graphite furnace
GFAAS	graphite furnace atomic absorption spectrometry

HA	hollow anode
HC	hollow cathode
HCL	hollow cathode lamp
HGA	heated graphite atomizer
ICC	integrated contact cuvette
ICP	inductively coupled plasma
ICP-OES	inductively coupled plasma optical emission spectrometry
LTE	local thermodynamic equilibrium
PMT	photomultiplier tube
rf	radio frequency
STPF	stabilized temperature platform furnace
T_e	electron kinetic temperature
T_{exe}	excitation temperature
TE	thermal equilibrium
T_g	gas kinetic temperature
T_{ion}	ionization temperature
v/v	volume - to - volume ratio
µL	micro litter

ACKNOWLEDGMENTS

I would like to express my deepest sense of gratitude and sincere appreciation to my research supervisor, Dr. M. W. Blades, Professor, Department of Chemistry, University of British Columbia, for his invaluable and scholastic guidance, constructive criticism, reviewing the manuscript and constant encouragement throughout the course of this project .

Special thanks to the various members of the research group, both for their beneficial discussions and their camaraderie - in particular Charles LeBlanc and Doug Weir.

Finally , I would like to thank my wife for her patience and encouragement during the course and preparation of this thesis.

CHAPTER 1

INTRODUCTION

Progress in many areas of analytical chemistry is made possible by technological development often based on advancements in fundamental scientific understanding. Analytical atomic spectroscopy is one of the important branches of analytical chemistry wherein the analytical spectroscopist develops, improves , characterizes, and then applies spectroscopic sources.

The main objective of the work described in this thesis was to characterize and to examine the stability of the radio frequency (rf) helium plasma source, operated at 13.56 MHz, in Furnace Atomization Plasma Emission Spectrometry (FAPES) as a spectrochemical source for elemental analysis.

This chapter is an introduction to FAPES and some special topics related to the work described in this thesis.

1.1 HISTORICAL DEVELOPMENT OF FAPES

The classic publication of Alan Walsh on Atomic Absorption Spectrometry (AAS), describing flame AAS [1], was a revolution for atomic spectrometric methods. As a result of this publication, flame AAS became the most widely

used spectrometric method for the determination of metallic elements, during the 1960's and 1970's. Even today, flame AAS is a useful method for a variety of analyses. Flame AAS has some common interferences, for example ionization , physical and chemical interferences, however these can be easily controlled.

The first systematic investigation of Graphite Furnace Atomic Absorption (GFAAS) was carried out in 1961 by L'vov [2] . Unlike the flame AAS method, wherein Walsh employed continuous nebulization of the sample into a flame to provide a steady state absorption signal, L'vov introduced a small sample volume, which was converted to an atomic vapor inside an electrically-heated graphite furnace. This graphite furnace method has very good detection limits for absolute amounts and there are very few atomic techniques which can successfully compete with those detection levels [3] .

For many years, GFAAS has been recognized as one of the most sensitive analytical techniques for elemental analysis [4]. On the basis of absolute mass, GFAAS detection limits are very low because sample volumes are small (5-100 µl), analyte transport efficiency is high (90-100%), and analyte residence time in the observation volume is relatively long (0.1-0.5 s). A limitation of GFAAS arises as a result of interferences. The interferences have been classified as interferences due to background absorption, condensed phase interferences, vapor phase interferences, and effects due to gas expansion [5-7]. The combination of a thermal pre-treatment step, temporal and spatial isothermal atomization through the use of stabilized temperature platform furnaces (STPF), rapid heating cycles, probe insertion, two-step furnaces, and background

correction techniques such as Zeeman, Smith-Hieftje and the use of continuum lamps have enabled sensitive determinations of a variety of complex samples. However, interferences continue to limit the effectiveness of GFAAS and, although the use of hollow cathode lamps as primary sources provides high spectral selectivity, they introduce the limitation that restricts GFAAS to being essentially a single element technique.

There was a flurry of interest in the spectrochemical application of capacitively coupled plasmas (CCP) in the late 1950s and early 1960s [8,9], but interest shifted to inductively coupled plasmas (ICP) in about 1964-1965 as a result of the landmark papers by Wendt and Fassel [10] and Greenfield *et al.* [11] describing Inductively Coupled Plasma Optical Emission Spectrometry (ICP-OES). Unlike the AAS method, emission spectroscopic methods such as ICP-OES are inherently multi-elemental techniques. The ICP is also relatively free from interferences since refractory oxides only partially dissociated in the flame are completely dissociated at high ICP temperatures. However, on a concentration basis, ICP detection limits are 10 to 100 times higher, and on an absolute basis, 1000 times higher than GFAAS [3].

A variety of approaches has been investigated for developing the graphite furnace into a source capable of carrying out simultaneous, multielement analysis [12]. The primary thrust behind these approaches has been to combine the excellent transport and residence time characteristics of the graphite furnace with some means of exciting the atomized analyte vapor inside the furnace. In this way atomic emission spectrometry (AES) can be used as a detection method. Littlejohn and Ottaway [13] have described carbon furnace

atomic emission spectrometry (CFAES) which is a sensitive technique for trace analysis using thermal excitation from normal furnace heating. However, this method is limited by the energy available for thermal excitation. For elements having resonance wavelengths below 300 nm, the detection limits are much poorer than those for GFAAS [14]. Furthermore, at temperatures above 2500 K, the intense emission from the furnace wall is a major source of spectral background in the visible region [15].

Falk and his co-workers [16-18] developed a furnace atomization non-thermal excitation source (FANES or HC-FANES). This source was based on using a low pressure, direct current (d.c.) glow discharge sustained inside a graphite furnace, which operated as a hollow cathode (HC) , and a point or ring external to the furnace as an anode. Figure 1.1 is a schematic diagram of the FANES source. The furnace was a Massamann-type and was graphite or pyrolytic-graphite coated graphite . Microliter volumes of sample was deposited onto the inner wall of the graphite furnace, and was vaporized into the discharge during a high temperature atomization step . Analyte atoms were excited in the discharge , emitting characteristic line spectra that could be used for simultaneous multi-elemental analysis.

It is well known that Penning and asymmetric charge transfer reactions are prevalent in low pressure plasma sources and this characteristic, coupled with collisions from energetic electrons, enabled the FANES source to excite atoms (and molecules) such that a wide variety of metals and non-metals could be determined (for example, with an absolute detection limit for Na of 0.0007 ng/ml [17]). An additional advantage to the FANES approach was that the atomization

and excitation processes were independent of each other and could thus be independently optimized. However, because of the low pressure requirement of the glow discharge operation, sample introduction is somewhat laborious and time consuming.

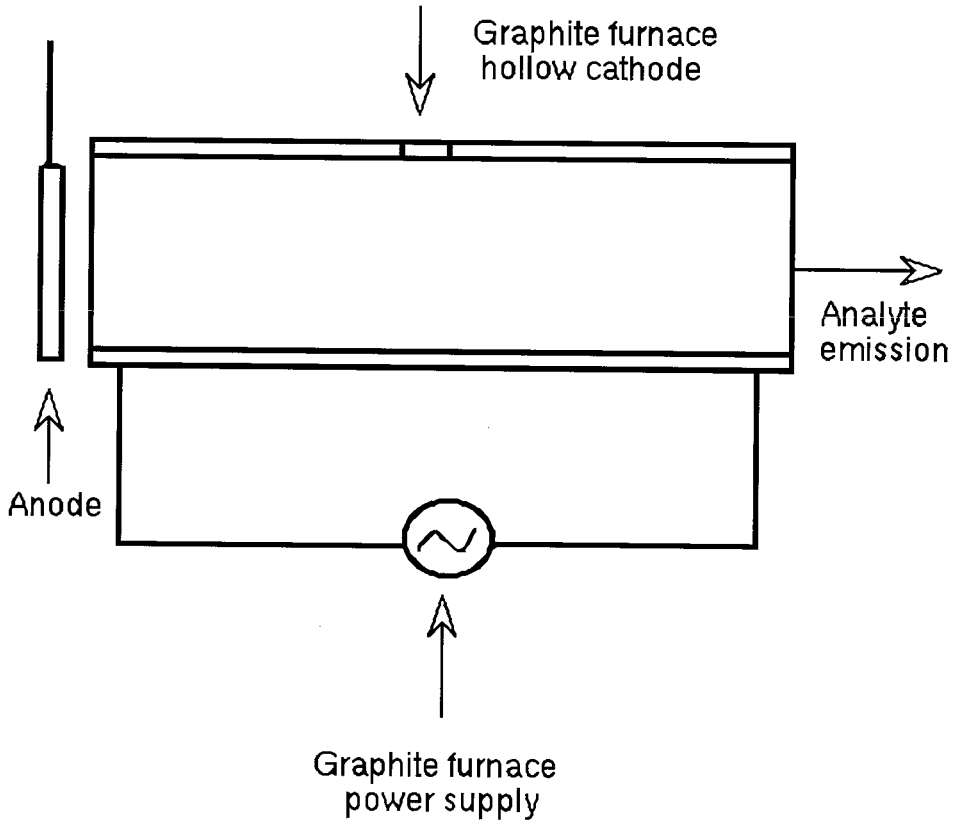

Figure1.1: Schematic representation of FANES source. (Adapted from H. Falk, E. Hoffmann and Ch. Ludke, Spectrochim. Acta, 283, 39B (1984), with permission of Pergamon Journal Inc.)

Ballou et al. [19-21] described a hollow-anode plasma excitation source which was conceptually very similar to the FANES source called HA-FANES. Figure 1.2 illustrates a schematic diagram of the HA-FANES source. For this source the graphite furnace formed the anode of a glow discharge and the cathode was a graphite rod which was oriented co-axially with the furnace and extended the entire length of the furnace. The graphite furnace was an integrated contact cuvette and the axial electrode was a pyrolytic-graphite coated rod. The rationale for this new design was that it simplifies electrical shielding requirements and enhances the reliability of operations. The operation of this source is similar to that of FANES and it suffers disadvantages similar to the FANES source with respect to operation at reduced pressure (<200 torr).

Liang and Blades first reported an atmospheric pressure radio frequency (rf) plasma source inside the graphite furnace for analyte excitation [22]. The geometric arrangement of the electrodes in the atmospheric pressure rf plasma was very similar to that of the electrodes in HA-FANES. The spectrometric method with such an rf plasma source has been designated Furnace Atomization Plasma Excitation Spectrometry (FAPES) [23,24]. Compared with low pressure operation, atmospheric pressure operation was expected to offer convenient sample introduction and increased residence time of analyte atoms within the graphite furnace [22]. The FAPES source, which can be maintained at frequencies of 13.56-50 MHz and rf powers of 5-600 W, is utilized to excite an atomic vapor produced from a normal graphite furnace atomization heating cycle. When coupled with a direct reading spectrometer the FAPES source could be used effectively as a means of carrying out simultaneous, multielement

determinations on small sample sizes in a manner similar to the use of GFAAS while maintaining similar detection sensitivity. A detailed description of FAPES is given in the next section.

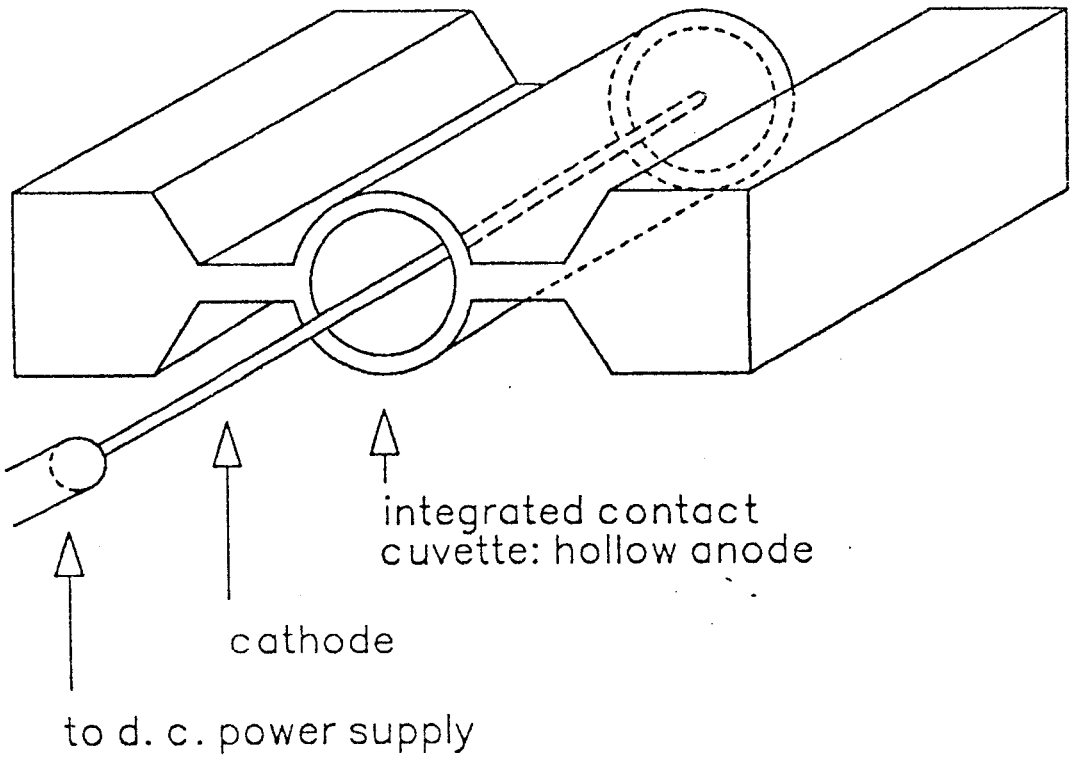

Figure1.2: **Schematic representation of HA-FANES source. (Adapted from N. E. Ballou, D. L. Styris and J. M. Harnly, J. Anal. At. Spectrom., 1141, 3, (1988), with permission of the Royal Society of Chemistry.)**

1.2 FURNACE ATOMIZATION PLASMA EXCITATION SPECTROMETRY

A schematic diagram of FAPES source described by Liang and Blades is shown in Figure 1.3 [22]. The plasma source consisted of a conventional Massmann-type graphite furnace work-head (modified Instrumentation laboratory, model IL 455), and a co-axial graphite electrode of 1 mm in diameter and 40 mm in length (Ringsdorff-Werke, FRG) connected to an rf connector. The rear optical window of the furnace work-head (through which light from the hollow cathode lamp is normally directed) was removed and replaced with an rf connector. The operating frequency was 27 MHz and the rf power delivered to the plasma was about 20 W, and helium was used as the plasma gas. Liang and Blades suggested that the mode of power coupling to the plasma was primarily capacitive in nature [22]. At first, Liang and Blades designated this plasma source an Atmospheric Pressure Furnace Capacitively Coupled Plasma (APF-CCP), however, this plasma source is now more commonly recognized as a FAPES by the acronym in the literature [25].

Liang and Blades tested the source using a small brass chip weighing about 5 mg. The emission spectra of Cu and Zn were recorded at 800 ^{o}C of furnace temperature with 20 W plasma power. They suggested that at low rf powers, the dominant sampling mechanism was rf sputtering [22]. A relatively high gas temperature and, as a consequence, a reduction in gas-phase chemical interferences compared with GFAAS, were expected for FAPES

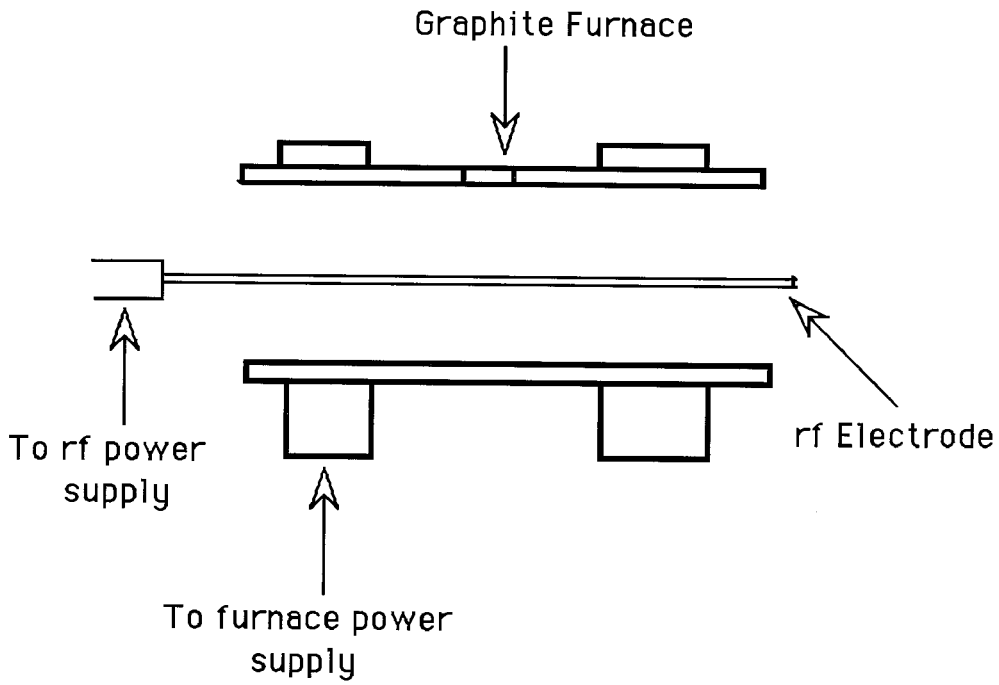

Figure1.3: **Schematic representation of FAPES source. (Adapted from D. C. Liang and M. W. Blades , Spectrochim. Acta, 1049, 44B, (1989), with permission of Pergamon Journal Inc.)**

Sturgeon et al. used a conventional Perkin-Elmer furnace (Model HGA-500) with a co-axial graphite rod [23]. External air was prevented from reaching the interior of the furnace by the positive pressure of the support gas through an internal flow through the furnace, which could be halted during the atomization cycle, and a continuous external flow around the furnace. The power delivered to the helium plasma was about 50 to 70 W. A 10 µl aliquot of test solution, containing Cd or Mn, was deposited on the furnace wall and subjected to the atomization cycle as in GFAAS. The plasma background emission and transient emission signals for Cd and Mn were given. The detection limits for Cd and Mn were 36 pg and 52 pg respectively.

1.3 ANALYTE ATOMIZATION

Sensitivity of atomic absorption or emission analysis varies with the fraction of the analyte atoms that are found in the light path or emit the characteristic wavelength at one time if peak height is being measured. If peak area is being measured, the sensitivity is proportional to the average residence time of the analyte atoms. An ideal atomizer would provide complete atomization of the element of interest irrespective of the sample matrix. For the lowest possible detection limits, at least for absorption the atomic vapor should not be highly diluted by the atomizer gas so that a large ground-state neutral atom population is produced.

1.3.1 Electrothermal Atomizer : The Graphite Furnace

With a graphite furnace a discrete sample is deposited and the furnace is electrically heated to produce a transient cloud of atomic vapor. To prevent the oxidation of graphite at high temperatures, the furnace is coated with a thin layer of pyrolytic-graphite during manufacture and purged with an inert gas.

The sample is placed on the furnace wall (wall atomization) or on a separate device inserted into the furnace (platform atomization). In the case of platform atomization, the platform is primarily heated by the radiation from the furnace wall. Typically, the furnace is heated in three stages in which the temperature of the furnace is increased progressively by passing larger currents through the

atomizer tube. The first step is drying or desolvation step, in which a sufficient current causes the furnace temperature to be increased and maintained at about 110 °C. During this stage, the solvent is evaporated leaving a solid residue in the furnace. The second step is ash step, in which the power supply current is increased, so that the furnace temperature is raised, typically to 350-1200 °C. During this stage, organic matter in the sample is ashed or converted to H_2O and CO_2, and volatile inorganic components are vaporized. The final step is the atomization step. During this stage the temperature of the furnace (atomization temperature) can reach a maximum as high as 3000 °C and the sample is vaporized and atomized to produce a atomic vapor cloud inside the furnace.

There are two kinds of non-flame atomizers which have received extensive experimental study. The first successful non-flame atomizer in the form of a carbon-rod electrode and a graphite furnace described by L'vov [2,26] is shown schematically in Figure 1.4. The graphite furnace was 30 to 50 mm long with an inner diameter of 2.5 to 5 mm. The furnace was heated up to about 2500 K. Sample was introduced into the furnace on a carbon rod electrode 6 mm diameter. The head of the electrode was shaped to fit an orifice in the wall of the graphite furnace. The graphite furnace was heated for 20 to 30 s and the electrode was moved into the orifice of the graphite furnace. Auxiliary electrical heating of the electrode was turned on for 2 to 3 s and absorption was measured. The electrode was then lowered away from the graphite furnace and the system was ready for the introduction of another electrode carrying the sample. To prevent penetration of the atomic vapor into the wall of the furnace, the inner wall was coated with a thin layer of pyrolytic-graphite.

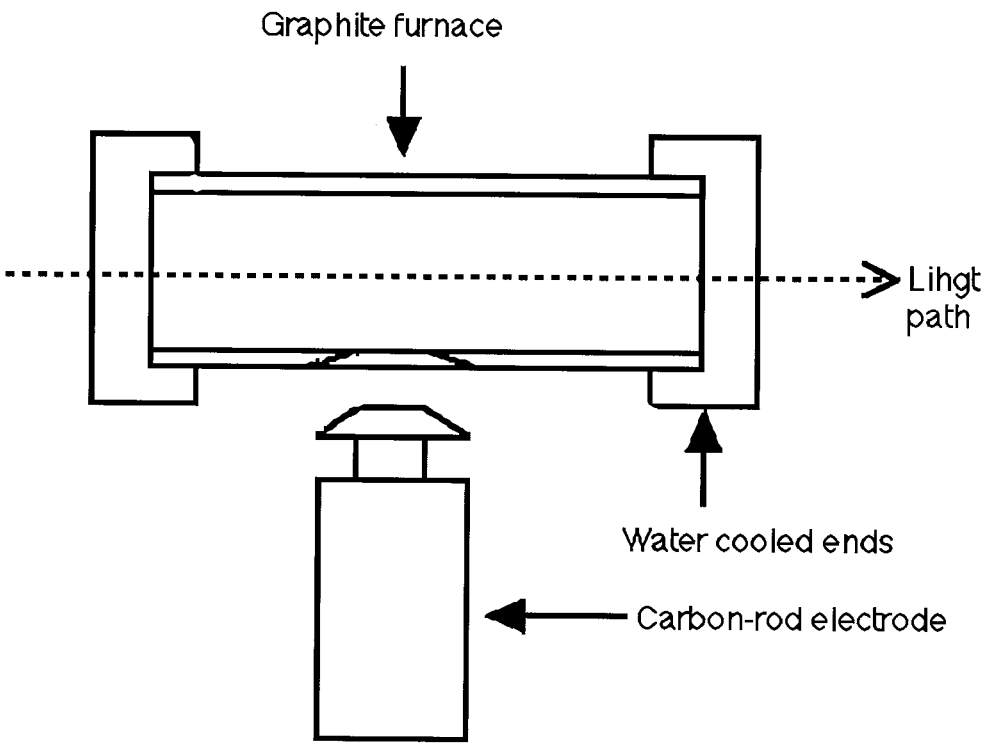

Figure1.4: **Schematic Representation of L'vov Furnace. (Adapted from B. V. L'vov, Spectrochim. Acta, 53, 24B, (1969), with permission of Pergamon Journal Inc.)**

Although the power to the furnace is stepped almost instantaneously to its selected value during the atomization step, it takes a finite time for the furnace temperature to reach its equilibrium value. When the wall of the furnace on which the sample is deposited reaches a critical temperature called the "appearance temperature", analyte vaporizes off the surface. The appearance

temperature depends on the analyte, the analyte concentration, and the sample matrix. The gas inside the tube is at a lower temperature than the furnace walls, so that atomized analyte atoms may suffer compound formation after vaporization. To alleviate these problems, L'vov was the first to employ a graphite platform installed inside the furnace from which the sample was vaporized rather than from the furnace wall [27]. This graphite platform is sometimes called the "L'vov Platform" or the "Stabilized Temperature Platform" (STPF) [28,29]. A schematic diagram of the L'vov platform is shown in Figure 1.5. The platform is heated primarily by radiation from the furnace during its heating cycle, so the temperature of the platform (and hence the sample temperature) lags the furnace wall temperature. Therefore, analyte vaporization and atomization are delayed until the gas-phase temperature within the furnace reaches the atomization temperature. In addition, due to the temperature difference between the furnace wall and the platform, a higher heating rate for the platform is achieved in the initial stages of the atomization step[27].

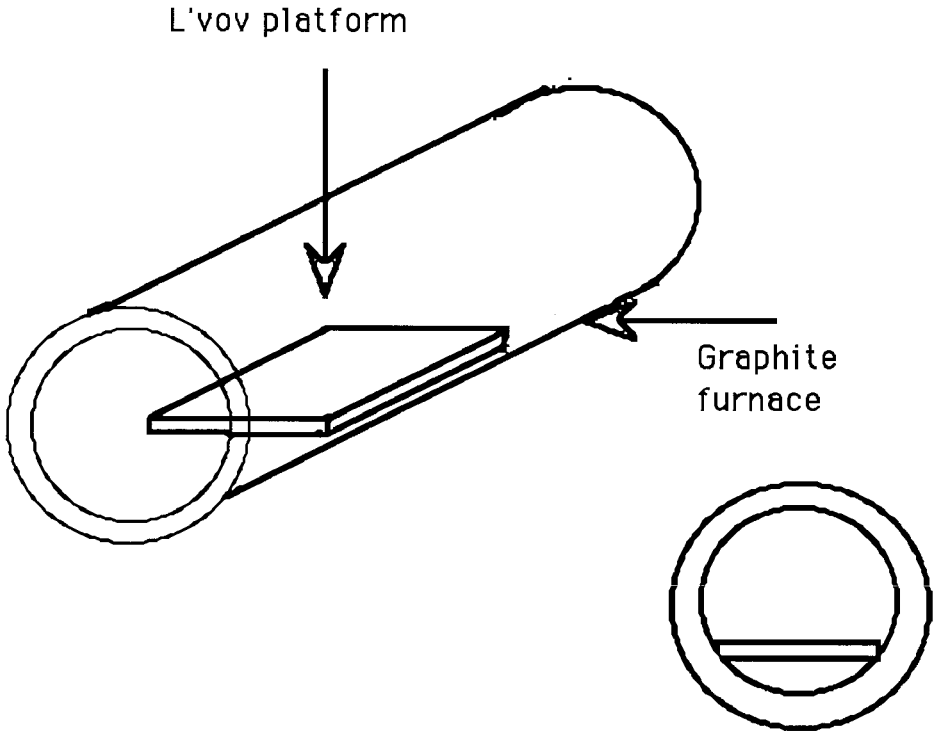

Figure 1.5: Schematic Representation of the L'vov Platform inside the graphite furnace.

Another successful non-flame atomizer is the Massmann furnace [30] shown in Figure 1.6. It is a simplified version of the L'vov graphite furnace. The Massmann furnace consists of a straight graphite tube of 55 mm in length, 6.5 mm in internal diameter and a wall thickness of 1.5 mm. The atomizer tube is supported at the ends by water-cooled electrodes. Liquid samples are deposited onto the inner furnace wall through a small hole in the center of the furnace by means of a micro-pipette, while solid samples were inserted from one side of the furnace. The temperature of the furnace could reach 2900 K

within a few seconds. The furnace was enclosed in a chamber and purged with Ar.

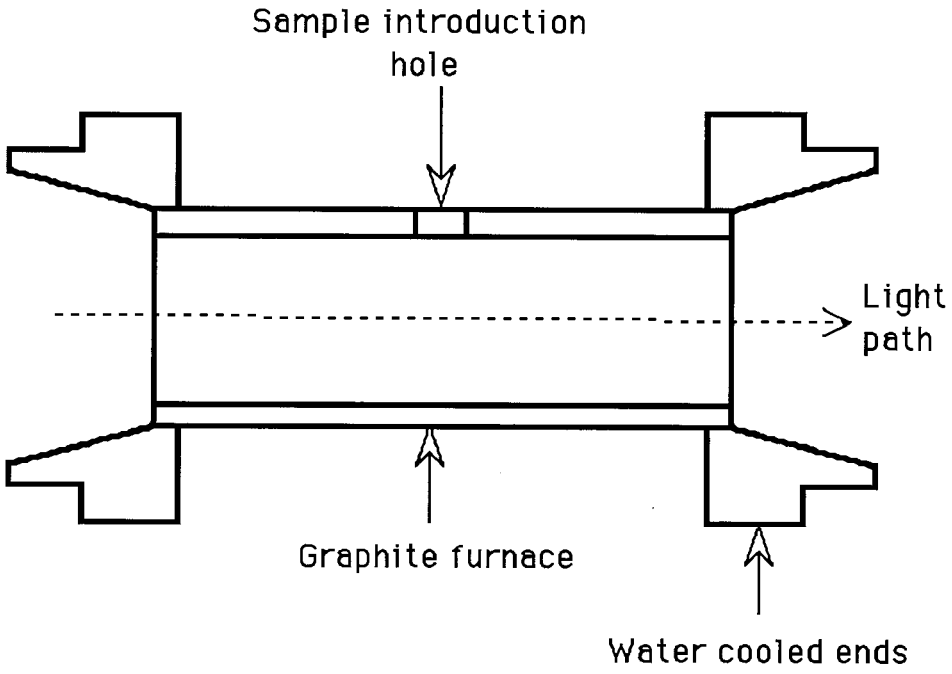

Figure 1.6 : Schematic Representation of the Massmann Graphite Furnace. (Adapted from H. Massmann, Spectrochim. Acta, 215, 23B (1968), with permission of Pergamon Journal Inc.)

Two major limitations are inherent in the Massmann-type furnaces, temporal non-isothermality and spatial non-isothermality [30]. Temporal non-isothermality occurs when analyte atoms appear in the observation volume during a time in which the temperature in the gas-phase is low and is changing rapidly. The atomization range within which atoms persist in the furnace (and hence the residence time of analyte atoms) is dependent on the nature of the analyte and

the accompanying matrix . As a result, the degree of atomization is often low and matrix dependent [27]. Spatial non-isothermality is the non-uniform temperature distribution along the furnace length and is caused by the heating characteristics of the water cooled ends of the furnace. This non-uniformity results in vapor condensation on the cooler end-regions of the furnace [25]. In addition, recombination of the sample vapor leaving the furnace through the cooler end-regions is a major contribution to spectral interferences in AAS [26]. Spatial non-isothermality of the furnace also has a severe effect in CFAES due to self-absorption [31].

Temporal non-isothermality can be removed by using L'vov platform with conventional end-heated Massmann-type furnaces but not the spatial non-isothermality. Spatial non-isothermality can be eliminated by employing a side-heated Integrated Contact Cuvette (ICC) [32]. In the ICC, the full length of the furnace starts to heat at the same time (transverse heating), and therefore, achieves spatial isothermality. All the work described in this thesis was carried out using an ICC type furnace.

1.3.2 Atomization in Graphite Furnace

Many studies on atomization mechanisms have been reported in the literature and various proposed mechanisms have been subjected to considerable debate over the years. The atomization mechanisms are very complex in nature and depend on the nature of the analyte, the accompanying matrix and, of

course, on the atomizer characteristics. When the analyte sample is in a nitric acid solution, the oxide of the analyte is formed from the nitrate during the ashing step or prior the atomization step. Some proposed atomization mechanisms are summarized below.

Mechanism I. Carbon Reduction

$$MO_{(s)} \xrightarrow[C]{\text{Reduction}} M_{(s,l)} + CO_{(g)} \xrightarrow{\text{Vaporization}} M_{(g)}$$

In this atomization process, the analyte oxide is reduced by carbon in the furnace wall to form analyte atoms either in solid or liquid form which are then vaporized to the gas phase.

Mechanism II. Thermal Dissociation

$$MO_{(s)} \xrightarrow[\text{Dissociation}]{\text{Thermal}} \underset{1/2\ O_2}{M_{(s,l)}} \xrightarrow{\text{Vaporization}} M_{(g)}$$

In this case, the analyte oxide dissociate thermally on the furnace wall followed by the vaporization of the analyte atoms.

Mechanism III. Dissociation of Oxide Vapor

$$MO_{(s)} \xrightarrow{\text{Vaporization}} MO_{(g,)} \xrightarrow{\text{Thermal}} M_{(g)} + 1/2\, O_2$$

Here, the analyte oxides vaporizes first from the furnace wall and followed by thermal dissociation producing analyte atoms in the gas phase. The gas-phase dissociation equilibrium of the analyte may be affected by the amount of oxygen which, in turn, is determined by the amount of CO in the gas-phase.

1.4 ANALYTE EXCITATION

For spectrochemical analysis, plasma discharges have been widely used during the past three decades. Plasma sources currently in use as spectroscopic sources include dc (Arc) and ac (Spark) plasmas, inductively coupled plasmas (ICP), microwave-induced plasmas (MIP), capacitively coupled plasmas (CCP), Capacitive microwave plasmas (CMP), glow discharges (GD), flowing afterglows, Theta-pinch discharges, exploding films and wires and laser-produced plasmas.

Without a doubt, the ICP is currently the most important plasma device used in the field of analytical atomic spectrometry. It has been successfully utilized as a source of atomic emission, absorption, fluorescence as well as the ion source for mass spectrometry. Capacitively coupled plasmas (CCP) at low pressure have been investigated extensively during the past couple of decades, mainly

because of their widespread use in plasma processing of semiconductors. However, this low pressure plasma discharge has been largely ignored by the analytical spectroscopy community mainly because of risk of contamination and difficulty of operation. Atmospheric pressure discharges are less prone to contamination and easier to operate. This was one of the main thrusts behind the development of atmospheric pressure CCP. The atmospheric pressure CCP operates using a variety of support gases including helium. This discharge is relatively simple to construct and operate; offer similar characteristics to microwave induced plasma (MIP); and in some cases inductive coupled plasma (ICP) and in many respects is much more versatile in terms of the mode of operation when compared with the other plasma discharges. Recently, rf discharge at low pressure has also been employed in mass spectrometry [33] and emission spectrometry [34].

1.4.1 : Atmospheric Pressure rf Discharge

When considering the electrode disposition with respect to the plasma discharge, there are basically two types of capacitively coupled rf discharge: those with one or more electrodes in contact with the plasma and those with electrodes isolated from the plasma by a dielectric wall, normally quartz or silica glass. Schwab at el. [35-38] have studied the properties of rf capacitive gas discharge at atmospheric pressure in which the electrodes were in contact with the plasma. He reported that these plasmas could operate in one of the two basic modes: glow discharge and arc discharge.

The type of plasma formed, arc or glow, depends on the type of material used for the electrodes, the condition of the surface, the current and the discharge gas. The two can be easily distinguished visually or from the current-voltage characteristics. The negative glow attaches to the negatively powered electrode but since the field is reversing rapidly both the electrodes exhibit a glow region.

For glow discharge, let us consider (for simplicity) two electrodes of equal area at a certain distance apart at low pressure. If a sufficient d. c. voltage is applied, a discharge strikes between the electrodes. In this discharge a cathode dark space and a glow can be seen. A cathode fall potential develops across the dark space, leaving the glow space nearly field free. For self-sustainment (current continuity) of the discharge, a steady state electron concentration must be maintained. In a d.c. glow discharge , this electron concentration is caused mainly by secondary emission through positive ion bombardment on the cathode.

If a low frequency alternating voltage is applied, instead of a d. c. voltage, the discharge behaves as though it has two alternating cathodes. This system is a succession of short-lived d. c. discharges, because at low frequencies there is ample time for the discharge to become fully extinguished. The discharge is extinguished when the cathode potential drops below the discharge sustain value because of the build up of a self-bias d. c. potential on the cathode. In the case of a d. c. discharge, the potential at the cathode is equal to the applied potential difference between the two electrodes but in an alternating current discharge, the d. c. potential at the electrodes is a self-bias voltage. This self-

bias voltage forms as a result of the differential mobility of electrons and positive ions in the discharge. Electrons collect on an electrode whenever the electrode becomes positive with respect to the glow space. Since capacitively coupled plasmas are operated using a capacitor connected in series between the driven electrode and rf power supply or impedance matcher called a blocking capacitor, the bias voltage does not bled away through the power supply.

If the frequency of the applied voltage is increased, it is observed that the minimum pressure at which the discharge sustains is reduced [39]. This reduction indicates that there is an additional source of ionization other than secondary electron emission from the electrodes. This additional source is resulted when electrons, oscillating in the time dependent electric field, undergo collisions with the plasma gas atoms to cause ionization. Therefore, the high voltage electrode that is necessary in a d. c. glow discharge for the secondary electron emission is not required to sustain the rf discharge [40]. Furthermore, the cathode glow attached to each electrode is the same as in the d. c. case.

In addition to the frequency of the discharge, the pressure is also an important parameter and affects the discharge characteristics in two ways. Firstly, in a low pressure discharge, the mean free path of the electrons and ions is long. The electric field in the cathode dark space causes the acceleration of positive ions through the dark space toward the cathode. These accelerated positive ions impinge on the cathode and cause sputtering of the electrode material and the emission of secondary electrons. However, at atmospheric pressure, the mean free path of the ions is short and therefore, ions can be

considered as stationary. Secondly, the high pressure discharge is essentially a low current glow discharge. Transition from glow to arc discharge can be produced by an increase in current under constant pressure (or by an increase in pressure at constant current) and a considerable fall in the discharge voltage which is associated with a change in the electron emission mechanism from the cathode [41]. In the case of an arc discharge, electron emission from the cathode is mainly thermionic and field emission.

In an atmospheric pressure discharge, a positive space-charge region is built up in front of the appropriate electrode in each negative half-cycle. At frequencies above 1 MHz, the length of this space-charge region does not exceed $5x10^{-3}$ cm (in air), neither does the mean free path of an ion [36]. The voltage of the rf discharge depends on the nature and the distance between the electrodes. The time scale of the application of the rf voltage is such that frequencies in the order of 1 MHz and above result in a pseudo-continuous plasma. The reignition voltage in each half cycle is dependent on the electrode distance. It has also been reported that the reignition voltage drops at a certain electrode distance [38]. This observed drop in the reignition voltage was attributed to the residual charge carriers at longer electrode distances and was not due to the space charge effect [38].

If the current density increases, an rf arc discharge can be observed which is brighter in appearance than a glow [35] and usually it does not maintain a stable position, but moves around on the electrode surface. The rf glow can turn temporary into an arc at any time. The transition to the arc is also favored by

conditions that facilitate electron emission, for example rough electrode surface and salt deposits. For analytical purposes, a glow discharge is preferred since excitation conditions are more uniform and stable, and hence the precision and accuracy should be superior. Figure 1.7 shows the main components of an rf discharge system which consists of an rf power supply, a matching network and the discharge.

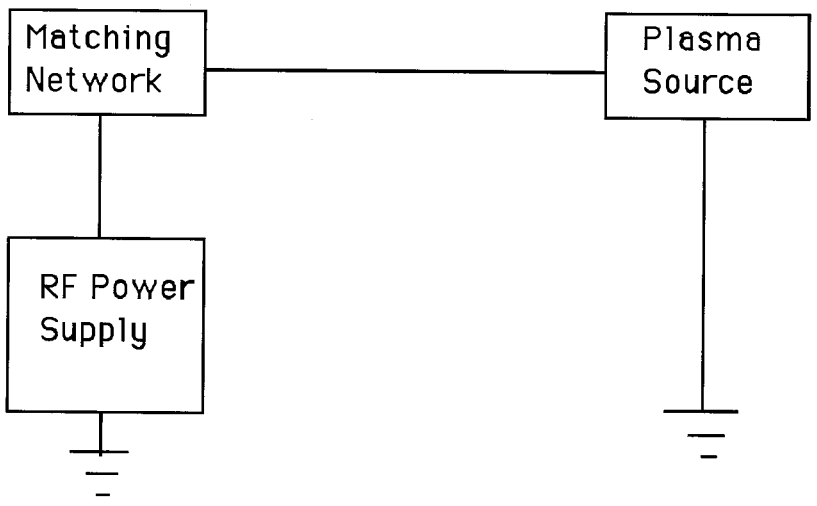

Figure 1.7 : Simplified Diagram of an rf Discharge System

1.4.2 The rf Discharge Characteristics in FAPES

The FAPES source enables the formation of He or Ar plasmas at atmospheric pressure inside an otherwise normal graphite furnace atomizer. The plasma is formed and sustained at atmospheric pressure by placing high voltage rf

excitation on a conductive electrode located inside the graphite furnace with a co-axial geometry, while maintaining the furnace at virtual ground. The plasma source within the graphite furnace is a bright region surrounding the rf electrode and a less intense plasma fills the remainder of the graphite furnace volume. It is also observed that when the rf power coupled to the plasma is increased, the bright region surrounding the electrode extends along the rf electrode beyond the length of the graphite furnace. The appearance of the extended rf glow along the rf electrode marks the onset of arcing between the rf electrode and the furnace wall. Voltage-current characteristics of the rf discharge in FAPES are not known yet and a mathematical model describing the discharge has not been developed.

It is interesting to note the use of rf discharge at atmospheric pressure in atomic spectrometry. Firstly, the discharge inside the graphite furnace is used only for the analyte excitation process. The analyte is introduced into the excitation volume during the high temperature atomization step of the furnace. Secondly, the discharge contains unequal electrode areas causing different current densities and electric field strengths on each electrode during each half-cycle. Therefore, this FAPES plasma source is not radially symmetric along the furnace length. Finally, the discharge contains hot electrodes with varying temperature up to about 3000 ^{o}C depending on the experimental conditions. However, depending on the rf power and the furnace temperature, the rf plasma appears to change into an rf arc with the evolution of the thermionic electrons.

1.4.3 : Plasma Temperature

The density of excited analyte atoms in a particular energy state in a source is determined by the dissociation equilibrium (Guldberg-Waage Distribution), population factor (Boltzmann Distribution) and degree of ionization (Saha Distribution). Temperature is the most important parameter governing the above equilibria. Temperature also changes the full-width of half-maximum (FWHM) of line profile which affects the sensitivity and linear dynamic range of a calibration curve for AAS. Both temporal and spatial isothermal operation is important for GF-AAS to obtain freedom from interferences, and to have high sensitivity, and precise analysis. Temperature is an important parameter in the control of the processes of diffusion, convection, and gas expansion. Furthermore, background intensity and signal-to-noise ratio are dependent on the temperature in the atomizer and source.

Relatively high temperature plasma sources such as ICPs give rise to intense line emission for the analyte and low matrix interference effects in the analytical determinations. This is why high temperature plasma sources are considered to posses superior analytical merit compared with those of low temperature plasmas. A unique temperature for a system can be specified only if the system is in a state of thermal equilibrium.

If thermal equilibrium is not established, a single temperature can not be assigned to the plasma. This non-thermal equilibrium leads to several different definitions of temperature in the plasma depending on the species considered which are : Electron Kinetic Temperature (T_e, from the Maxwell velocity

distribution), Gas Kinetic Temperature (T_g, from the Maxwell velocity distribution) Excitation Temperature (T_{exe}, from the Boltzmann energy state distribution) and Ionization Temperature (T_{ion}, from the Saha equation). However, when the source is in a state of local thermodynamic equilibrium (LTE), a unique temperature can be defined for each point in the source but allowing for the possibility of different temperatures at different points. A more comprehensive description of plasma temperatures and the relevant distribution functions are available elsewhere [42, 43].

1.5 OVERVIEW OF THESIS

The work described in this thesis is focused on further characterization of Furnace Atomization Plasma Excitation Spectrometry as a spectrochemical source for elemental analysis. In the next chapter a brief description of the experimental system used for this thesis is given. This experimental system can be used to acquire two data channels simultaneously.

Chapter three deals with the investigation of the plasma stability. The emission behavior of a He (I) and CO^+ line are studied at different rf powers. Reflected power for different forward rf powers are measured. The effect of thermionic electron emission and furnace wall temperature on the rf plasma are also discussed in this chapter .

Spatial and temporal emission characteristics of the rf plasma for Ag are discussed in chapter four . Both atomic absorption and emission are measured to study the effect of rf power on the temporal response of the analyte emission signal . The effect of rf power on integrated emission signal and the quenching of plasma at higher rf power is also discussed in this chapter .

In chapter five, the conclusions are presented, some limitations are pointed out and some recommendations are made to improve the present instrumentation of FAPES .

CHAPTER 2

EXPERIMENTAL SYSTEM

An experimental system capable of measuring simultaneous atomic emission and atomic absorption was used to study the plasma stability for FAPES as well as to study the time-resolved and spatially-resolved behavior of the analyte. A brief discussion of instrumentation, data acquisition, data processing and as well as experimental method for FAPES is presented in this chapter.

2.1 INSTRUMENTATION

A schematic diagram of the experimental system is depicted in Fig. 2.1. The main components of the FAPES source assembly were an rf power supply, an rf matching network, a plasma source work-head, and a furnace power supply for resistance-heating the graphite furnace. In addition, two lenses (L1 and L2), a monochromator, a photomultiplier tube (PMT), and a current amplifier were used for the spectral isolation and detection along with an analog-to-digital converter (ADC) and a computer (PC/AT) for the data acquisition.

In figure 2.1 the ADC data channels are labeled as C1 and C2. When the atomic absorption signal was measured, a lock-in-amplifier was employed to detect the hollow cathode lamp (HCL) signal from the PMT output. For other

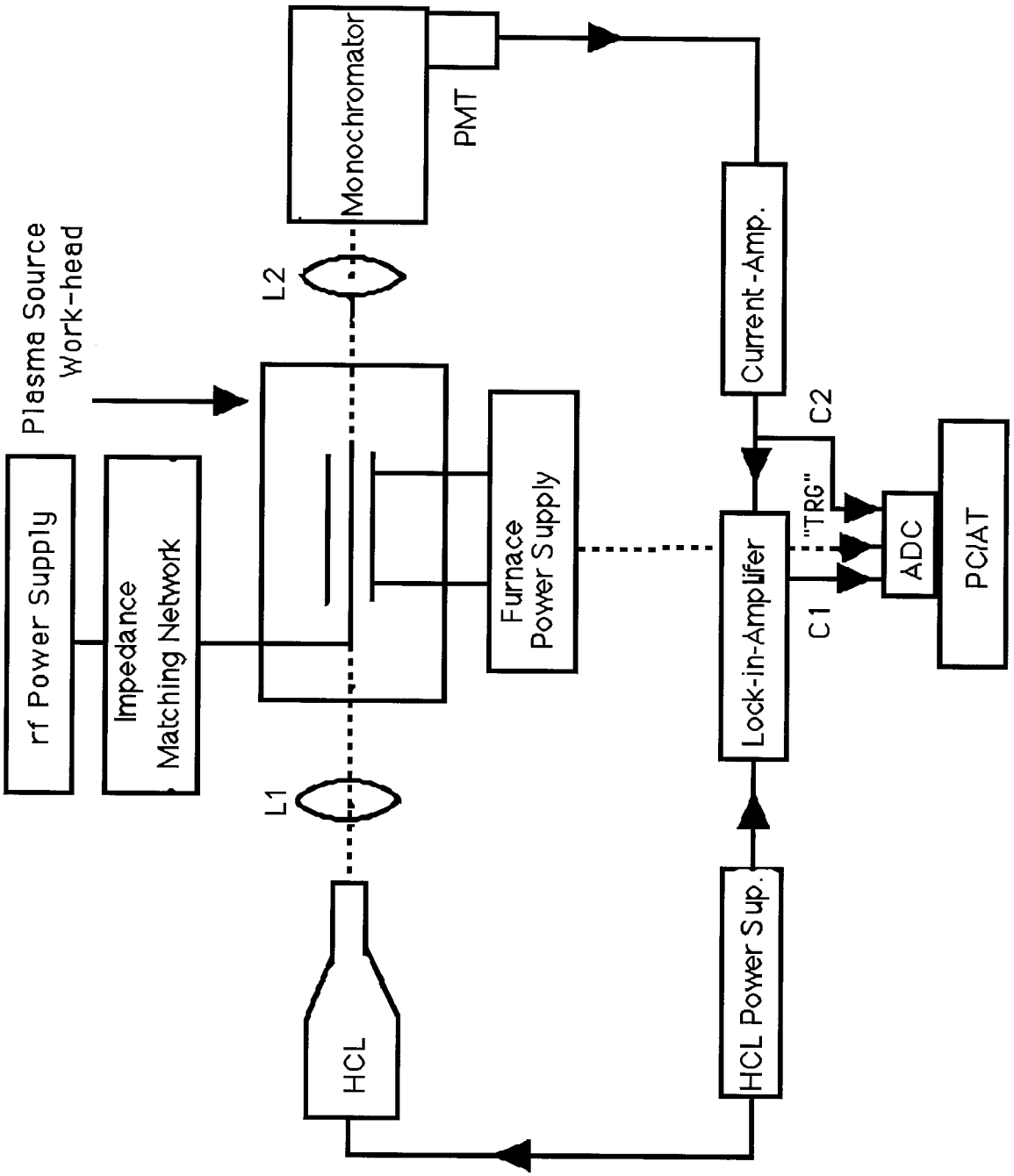

Fig. 2.1: A Schematic Diagram of the Experimental System

experiments, C1 was connected to the output from the corresponding signal transducer, for example ; optical pyrometer , to acquire the data. The "TRG" in the figure represents the trigger channel for the ADC.

2. 1. 1 The Plasma Source Work-Head

A schematic diagram of the plasma source work-head is depicted in Fig. 2.2. The work-head was a five-way hollow cube made of aluminum containing a pyrolytic-graphite coated integrated contact cuvette (ICC), a tungsten co-axial rod, and a high current furnace support structure made of copper and Macor^{TM}. The hollow five-way cube was 6 x 6 x 6 inch with 5 inch diameter "O"-ring sealed aluminum flange. The ICC was 19 mm long, 5.7 mm in internal diameter and 7.1 mm in outer diameter. The co-axial rod was 0.9 mm in diameter and extended up to the full length of the graphite furnace.

The furnace support structure and the water cooling system of the graphite furnace were similar to the method described by Ballou *et al.* [19].The graphite furnace was resistance-heated by using a furnace power supply (Model IL-655, formerly Instrumentation Laboratory; now Thermo-Jarrell Ash, Waltham, MA, USA). The plasma gas was directed into the work-head through a small inlet on the flange with the furnace support system and out through a small outlet located on the opposite flange.

The co-axial rod was attached to the rf connector using a "vertical mount", where it was powered using two vertical metal blades (as in Figure 2.2). This kind of arrangement is suitable for simultaneous measurements of absorption

and emission signal. The alternative arrangement, when the co-axial rod is directly connected to the rf connector in line is called the "horizontal mount".

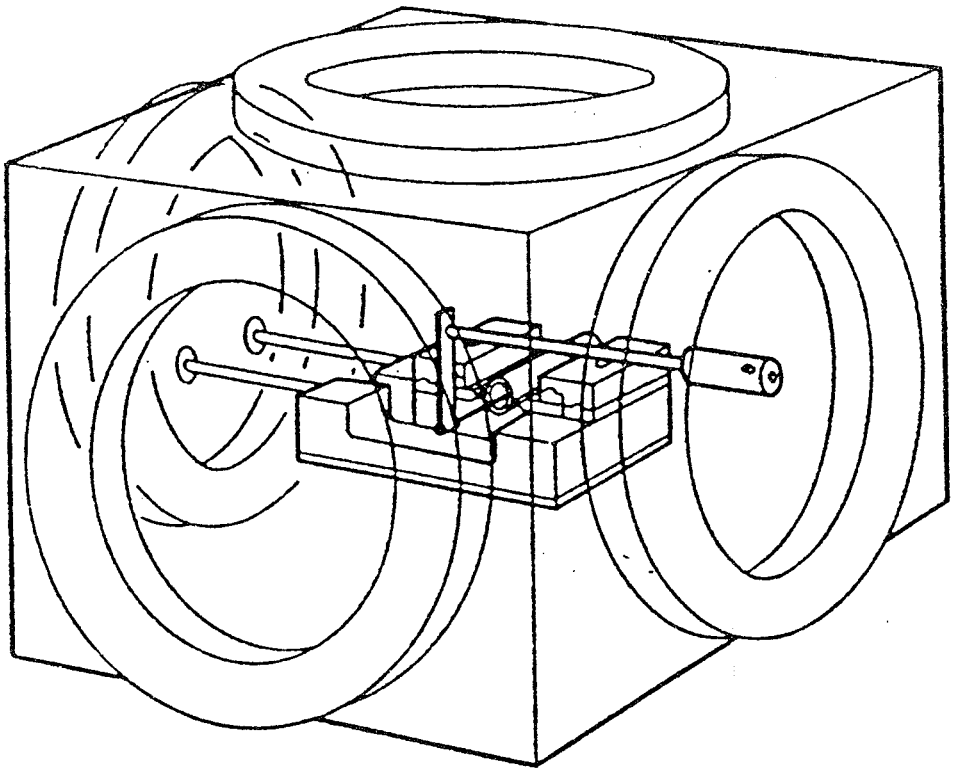

Figure 2.2: Schematic Diagram of the Plasma Source Work-Head

The plasma was viewed through a one inch diameter quartz window on the front-side flange. On the opposing backside, a similar quartz window allowed a light source (hollow cathode lamp) to be directed through the graphite furnace for atomic absorption experiments, or a horizontal-mount can be installed instead of the quartz window if necessary. The analyte sample was deposited

onto the inner furnace wall through a small screw-top port mounted on the top flange.

2. 1. 2 The Atmospheric Pressure rf Discharge

Inside the graphite furnace, a helium gas discharge was sustained by employing a 13.56 MHz rf generator (Model RFX-600, Advanced Energy, Fort Collins, CO, USA), an automatic power tuner (Model ATX-600, Advanced Energy, Fort Collins, CO, USA) and an impedance matching network (Model 5017-000-G, Advanced Energy, Fort Collins, CO, USA). The rf electrode was coupled with the output of the matching network through a variable 1-10 μH inductor. With this arrangement a helium discharge over the power range between 10 and 150 W could be ignited and sustained. At an rf power above 50 W, occasional arcing was observed between the rf electrode and the furnace wall.

2. 1. 3 Spectral Isolation and Detection

A 0.35 m Czerny-Turner monochromator (Model 270, Schoeffel-MacPherson, MA, USA) with a holographic grating of 2400 lines/mm was used for spectral isolation. The entrance slit of the monochromator was 50 μm wide. Signals were detected with a photomultiplier tube (PMT, Model R955, Hamamatsu, Middlesex, NJ, USA).The PMT was operated at 700 V. The output of the PMT was amplified using a current amplifier (Model 427, Keithley, Middlesex, NJ,

USA). The gain and the rise time of the current amplifier was 10^7 and 0.3 ms respectively, unless otherwise noted.

For atomic absorption experiments, a 1 : 1 image of the hollow cathode light was formed at the center of the furnace by using a 20 mm diameter, 75 mm focal length fused silica lens (L1; Melles Griot, Irvine, CA, USA). Another 1 : 1 image of the furnace plasma was formed at the entrance slit of the monochromator by using a 50 mm diameter, 150 mm focal length fused silica lens (L2; Melles Griot, Irvine, CA, USA). The plasma source work-head, furnace and the hollow cathode lamp (when necessary) was aligned with the entrance slit of the monochromator by using a HeNe laser (Melles Griot, Irvine, CA, USA).

2. 1. 4 Measurements of Spatially Resolved Intensity

The plasma source work-head was mounted on a post which in turn was mounted on a crank-driven linear translation platform. This platform allowed the work-head to be moved literally relative to the detection system. For spatially resolved emission intensity measurements, the work-head was translated in increments of 0.25 mm. A displacement indicator gauge (Model 2047-11, Mitutoyo, Japan) was used to monitor the platform movement precisely.

2. 1. 5 Temperature Measurements of Graphite Furnace

The temperature of the graphite furnace was measured my monitoring the radiation emitted from the furnace during the atomization step. The emission of the radiation was monitored by using an optical pyrometer (Ircon Series 1100, Model 11 x 30, IL, USA) which viewed the sample introduction hole through a 1 inch diameter quartz window on the top flange of the work-head. The optical pyrometer was mounted on a support-arm which in turn was fixed to the plasma source work-head by a vertical post. The pyrometer could be rotate around the vertical post which allowed it to be focused onto a selected position on the graphite furnace.

The pyrometer output was amplified by an amplifier (Electrical Services Shop, Department of Chemistry, UBC) and then digitized. The digitized data were converted into absolute temperature by using the calibration data provided by the pyrometer manufacturer and fitted to a 8 th order polynomial least square fit. The graphite furnace was assumed as a gray body radiator with an emissivity of 0.7.

2. 1. 6 Measurement of Atomic Absorption

During the measurement of atomic absorption, the output of the current amplifier was fed into a lock-in-amplifier (Model 121, PAR, Princeton, NJ, USA) as input signal. The reference signal of the lock-in-amplifier was from the HCL source which was modulated at 200 Hz by using a pulsed power supply (Electrical Services Shop, Department of Chemistry, UBC). This pulsed power supply can

be modulated up to 500 Hz and can deliver up to 100 mA of current. The output of the lock-in-amplifier was passed to a data acquisition system through channel number 1 (C1). The output was saved and absorbance was calculated.

2.2. DATA ACQUISITION AND PROCESSING

The graphite furnace supply triggered the analog-to-digital-converter (ADC) by a trigger signal as soon as it started the atomization step, to start the data acquisition. The signal from the single or two channels was digitized with 12-bit resolution by using a sixteen channel ADC (Model ADM12-10, Quatech, Akron, OH, USA). The ADC was capable of operating at a maximum sampling rate of 30 KHz. The data were stored by using a 12 MHz IBM PC/AT compatible computer.

The data acquisition software allowed two signals, analyte and background, to be acquired and stored in the computer. The data acquisition rate (maximum of 250 Hz) and the number of data points per channel (maximum of 2000 points) were software selectable and were limited by the free conventional memory allocated by the version 4.0 of MS-DOS™.

The data processing software facilitated the calculation of diagnostic information such as peak height, peak area and the peak width of the temporal response of the emission signal. It also calculated the absorption from the HCL signal. Other options included were background correction, signal averaging, smoothing, displaying and generating plots for the HP™ plotter.

2. 3. EXPERIMENTAL METHOD FOR FAPES

The analyte sample or the blank solution was deposited onto the furnace wall using an eppendorf digital pipette (Model No. 4710. Eppendorf, German) and was subjected to the thermal treatment. The furnace temperature program was in auto mode and the duration of heating steps were selected. After the ashing step there was 10 s lag. Within that lag the rf power was applied to the rf electrode, and the plasma was ignited. This lag allowed sufficient time to ignite, and to stabilize the plasma before the start of the atomization step. At the beginning of the atomization step the data acquisition was automatically triggered. The minimum atomization step was limited to 5 s by the furnace power supply and the signals were collected for 8 s. The cooling of the graphite was the next step after which the system was ready for the next sample. The sufficient cooling of the furnace support structure, made of copper, during the atomization step and removal of the hot gases from the plasma source work-head after the atomization step were two important considerations for the usable atomization temperature with this experimental system. The sample throughput was 4 to 6 samples per hour.

CHAPTER 3

INVESTIGATION OF THE PLASMA STABILITY USING He(I) AND CO^+ EMISSION LINE AND REFLECTED POWER MEASUREMENTS

3.1 INTRODUCTION

Discharge stability is one of the most important considerations for the successful utilization of a plasma source in emission spectrometry. In addition , for FAPES , the furnace temperature is an important fundamental property which is closely associated with analyte atomization and excitation . In high temperature plasmas, analytes produce intense atomic or ionic line spectra that can be used for analytical determinations. The emission intensity of an analyte depends on the total number of atoms or ions in the volume from which the signal is collected and the fraction of atoms or ions that are in the excited state.

In this study, the stability of the He plasma source at 13.56 MHz in FAPES was investigated. Temporal profiles of the He (I) line, CO^+ line, and the reflected power as a function of temperature are presented in this chapter.

3.2 CALCULATION OF THERMIONIC EMISSION FROM GRAPHITE

During the atomization cycle , the temperature of the furnace wall becomes high enough (2200 K) to emit thermionic electrons. The effect of thermionic electrons on the properties of the plasma discharge and on the analyte signal is not known at this time.

The phenomenon of thermionic emission is related to the ejection of electrons or positive ions from a solid when it is heated to a sufficiently high temperature. The current density, j, of electrons emitted from a uniform surface of a pure metal can be expressed in terms of the metal temperature, T, by Richardson equation [44]

$$j = A\,(1 - r)\,T^2 e^{-e\phi/kT}$$

In this equation A is a constant which is the result of a combination of fundamental physical constants

$$A = 4\pi m k^2 e h^{-3} = 120 \text{ amp. cm}^{-2}\text{. deg}^{-2}$$

where e is the absolute value of the electron charge, k is Boltzmann's constant, and h is the Planck's constant. r is the reflection coefficient for electrons crossing the potential barrier at the metal surface when the electric field just outside the metal is zero. For pure metals, r is around 0.05. ϕ is usually called the electronic work function and is defined so that ϕe is a characteristic amount of work required to remove an electron from the interior of the metal to a position just

outside the metal surface. In general, ϕ is dependent to some extent on temperature and the normal component of the electric field at the metal surface.

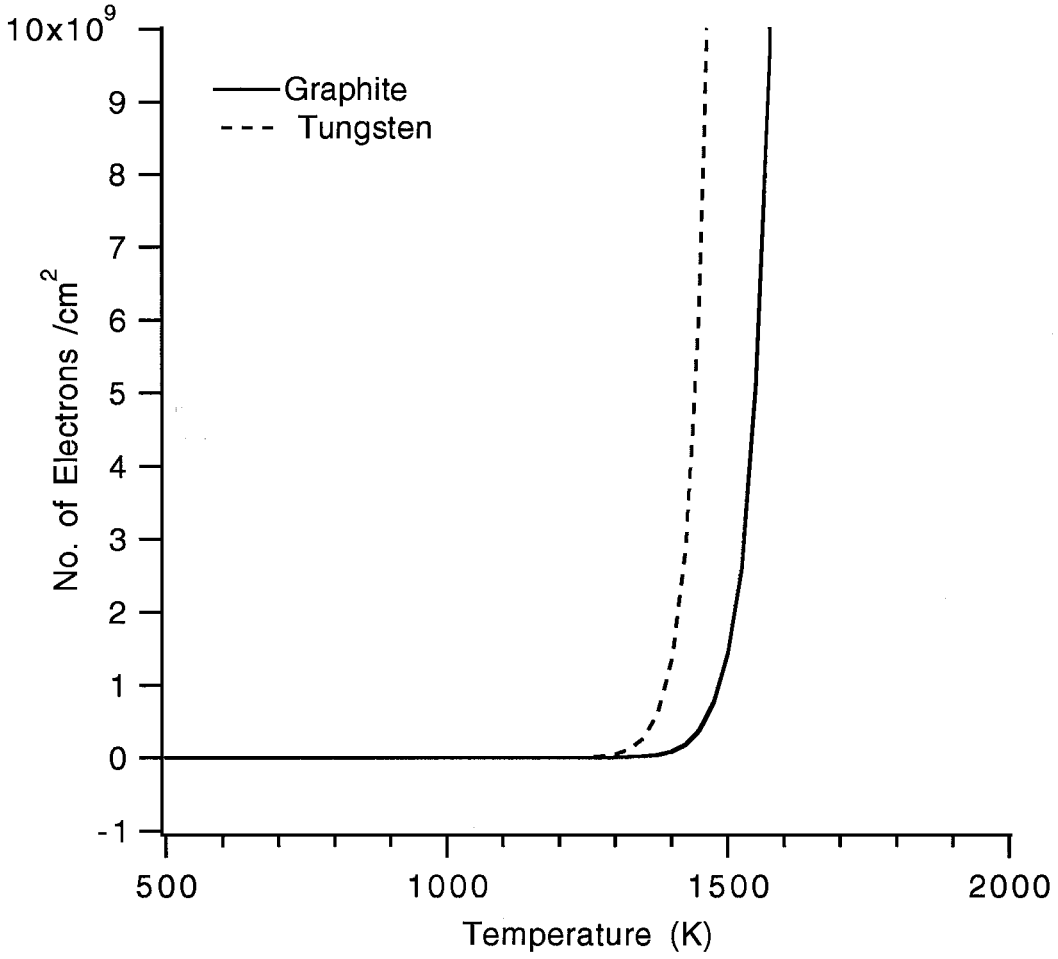

Figure 3.1. **Electron flux for graphite and tungsten as a function of furnace wall temperature.**

A calculation of electron emission from graphite and tungsten was done at different temperature and is plotted in Figure 3.1. The calculation was carried out using Richardson equation and using the work function of graphite is 5 eV and that of tungsten is 4.55 eV . The figure shows the variation of electron flux with temperature where the number of electrons increases exponentially with temperature for both graphite and tungsten. In the case of graphite (having higher work function), the exponential increase of electron flux happens at a higher temperature than for tungsten (having lower work function).

In the case of FAPES , the emitted electrons from the graphite furnace wall and from the graphite (or tungsten) electrode may change the power coupling efficiency between the load impedance and output impedance of the rf oscillator. The alteration of impedance matching may change the plasma characteristics and may even cause plasma shut-off (Sections 3.4.1 and 3.4.2). Thermionic emission from the furnace wall and the rf electrode may also causes an increase in reflected power (Section 3.4.3).

3.3 EXPERIMENTAL

The experimental system described in Chapter 2 was employed in the present study. The plasma source work-head was a Massmann type fitted with a pyrolytic-graphite coated rf electrode [22]. This furnace work-head was used to collect spectra without ingress of atmospheric gases when it was purged and

sealed effectively. This source was operated at rf powers of 25, 50, 75 and 100 W.

A 0.35 m Czerny-Turner monochromator (Model 270, Schoeffel-McPherson, MA, USA) equipped with a holographic grating with 1200 lines/mm was used for the measurement of the He and CO^+ line spectra from the plasma source. The 1:1 image of the plasma was formed at the entrance slit of the monochromator by using a fused silica lens (Oriel, Stratford, CT, USA) with 150 mm focal length and 50 mm diameter. Measurements of the plasma reflected power levels were obtained from the appropriate I/O port on the rear of the RFX-600 rf power supply (Advanced Energy, Fort Collins, CO, USA).

A PMT (Model R955, Hamamatsu, Middlesex, NJ, USA) was used as a detector. The output from the PMT was amplified by using a current amplifier (Model 426, Keithley, Middlesex, NJ, USA). The amplified signal was converted to digital form by using an ADC (RC Electronics, Santa Barbara, CA, USA) and stored in a 12 MHz IBM PC/AT compatible computer for further processing. The data acquisition was accomplished by the software provided by RC Electronics Co.

3.4 RESULTS AND DISCUSSION

3.4.1 Emission Spectra for CO^+ line

With a helium plasma source, the dominant background emission spectra are from CO^+, OH, NH, N_2 and N_2^+ and He. In the 220 to 270 nm region , the spectra are dominated by emission bands of CO^+ [45]. It is well known that CO^+ is readily excited in a helium discharge as a result of selective excitation according to the following reactions [46] ;

$$He^+ + 2He \longrightarrow He_2^+ + He$$

$$He_2^+ + CO \longrightarrow CO^+(B\,^2\Sigma^+) + 2He \quad \text{(Charge Transfer)}$$

$$He(2\,^3S) + CO \longrightarrow CO^+(A\,^2\Pi) + e + He \quad \text{(Penning Ionization)}$$

The potential energy range of He_2^+ (18.3 - 20.3 eV) is mainly responsible for excitation of CO^+ ($B\,^2\Sigma^+$) state by a resonant charge-transfer mechanism [47] .

Typical emission intensities for CO^+ line at 219 nm for different plasma powers at 13.56 MHz are provided in Figure 3.2. Four replicate measurements were carried out for each determination. These were then averaged and presented in the Figure. The variation of emission intensity for CO^+ was measured by a non-sample (no aqueous sample was deposited) atomization step in order to examine the effect of furnace wall temperature on the CO^+ emission intensity. The furnace wall temperature was measured

simultaneously using an optical pyrometer (Ircon Series 1100, Model 11 x 30, IL, USA). In the figure, the temperature axis does not represent the actual wall temperature for the first 2.4 second and from 5th to 6.4th second of the atomization cycle due to the pyrometer sensor used during the experements.

At this time, it is not clear whether the oxidation of carbon from the rf electrode and furnace wall, or desorption of carbon from the rf electrode and from the furnace wall is the major source of carbon in the gas-phase. However, in an atmospheric pressure helium plasma, it is most likely that CO^+ is mainly formed from CO which results from the oxidation of carbon , by residual O_2 in the gas phase. The gradual degradation of the rf electrode is the evidence of this process. The formation of CO, in the presence of a plasma, is an additional source of CO which is not found in GFAAS.

As seen in the figure, there is a small increase in the emission intensity at the very beginning of the atomization step (around 1260 K), followed by a depression and then a dramatic increase in the emission intensity which is again starts to depress dramatically at a furnace wall temperature around 1450 K . This complex response of the signal may be due to random variation of the amount of CO^+ in the furnace during the different stages of the atomization cycle. The initial increase in the emission intensity is most likely due to increase in the amount of CO in the plasma as a result of increased desorption of CO from the rf electrode and the furnace wall. The density of thermionic electrons from the heated rf electrode and furnace wall increases with the furnace wall temperature . These thermionic electrons might recombine with CO^+ and

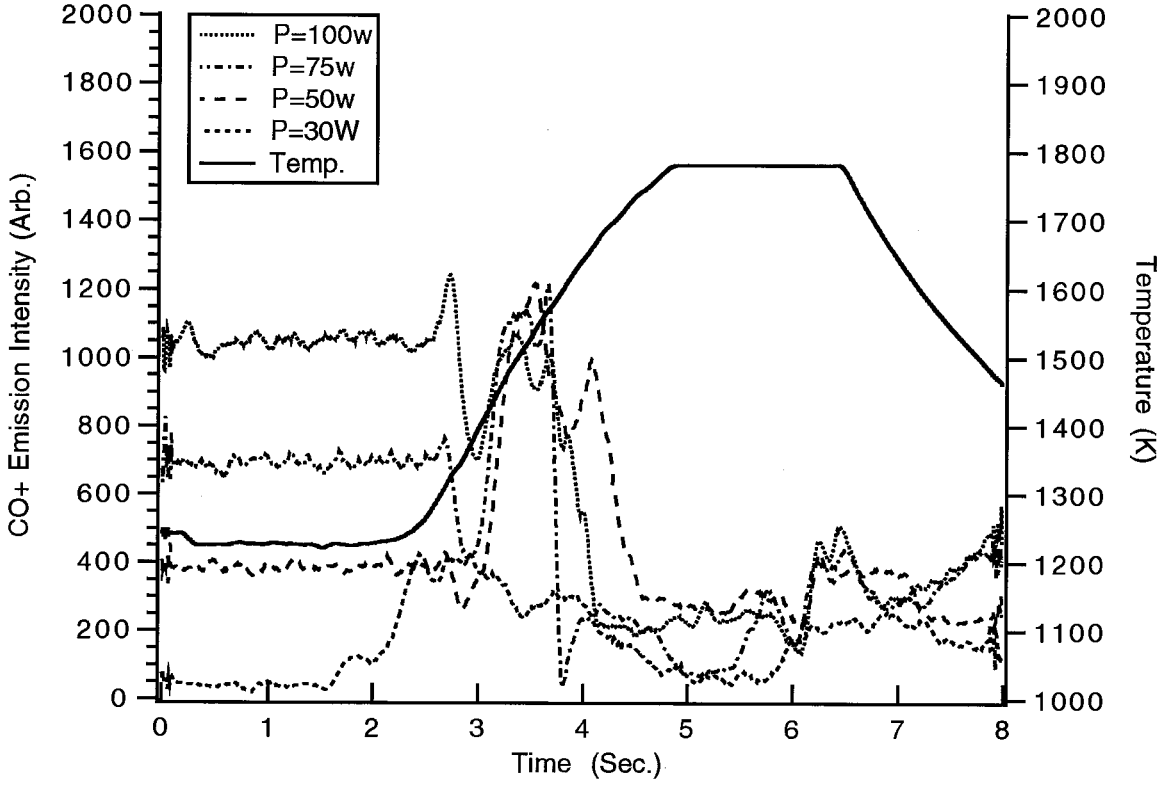

Figure 3.2. **Temporal emission behavior for CO^+(219 nm) at rf power of 30, 50, 75 and 100 W and time-temperature profile for furnace wall .**

be responsible for the depression of CO^+ emission intensity. This observed depression may also be due to the recombination of He_2^+ with the thermionic electrons, and hence, change in the excitation characteristics for CO^+. At high temperature region, the rapid changes of furnace wall temperature might cause the change of power coupling efficiency between the load impedance and output impedance of the rf oscillator. This alteration of impedance matching

could shut-off the plasma, and, hence decrease the CO^+ emission intensity dramatically.

3.4.2 Emission Spectra for He(I) line

The emission of He (I) lines at 388.8 nm for a 50 W plasma (frequency was not given) [23] and at 388.8, 447.1, 471.3, 492.2 and 501.6 nm for a 50 W plasma at 13.56 MHz [48] were reported by Sturgeon *et al.* . In a subsequent publication, some He (I) lines (447.1, 471.3, and 492.2 nm) observed for a 13.56 MHz helium plasma [48], were absent in the helium plasma at 40 MHz [49]. Hettipathirana *et al.* also reported the emission of He (I) line at 501.6 nm for a 16 W, 18 W, 22 W, 26 W and 30 W plasma at 13.56 MHz [45].

A typical temporal emission intensity for He (I) line at 501.6 nm for different plasma powers at 13.56 MHz is provided in Figure 3.3. Four replicate measurements were carried out for each determination which was then averaged and presented on the Figure. The variation of emission intensity for He (I) was measured by a non-sample (no aqueous sample was deposited) atomization step in order to examine the effect of furnace wall temperature on the He (I) emission intensity as well as to determine the stability of He plasma with furnace wall temperature. The furnace wall temperature was also measured simultaneously.

From the Figure 3.3 , it is clear that there is an increase in the emission intensity at the beginning of the atomization step with increasing rf power. This increase in the helium emission is due to the increase in excitation when the rf power is increased. For each rf power there is also an initial increase in the emission intensity with increasing furnace temperature. This increase might be because of change in the He-excitation temperature. However, Sturgeon *at el.* reported that, for a 100 W plasma, the He-excitation temperature was unaffected by the furnace wall temperatures between 500 and 2500 K [50].

Figure 3.3 also shows that the initial increase in the emission intensity followed by a dramatic decrease in emission intensity which is dependent on rf power as well as on furnace temperature. For higher rf power, the decrease in intensity appears earlier (in terms of time and temperature) than that for the lower rf power. This dramatic decrease happens at around 1375 K for rf power 30 W and 1200 K for rf power 100W. After the dramatic decrease the behavior of the helium intensity is random and inconsistent. When the atomization cycle is over, the furnace wall temperature starts decreasing and the helium emission intensity begins to increase .

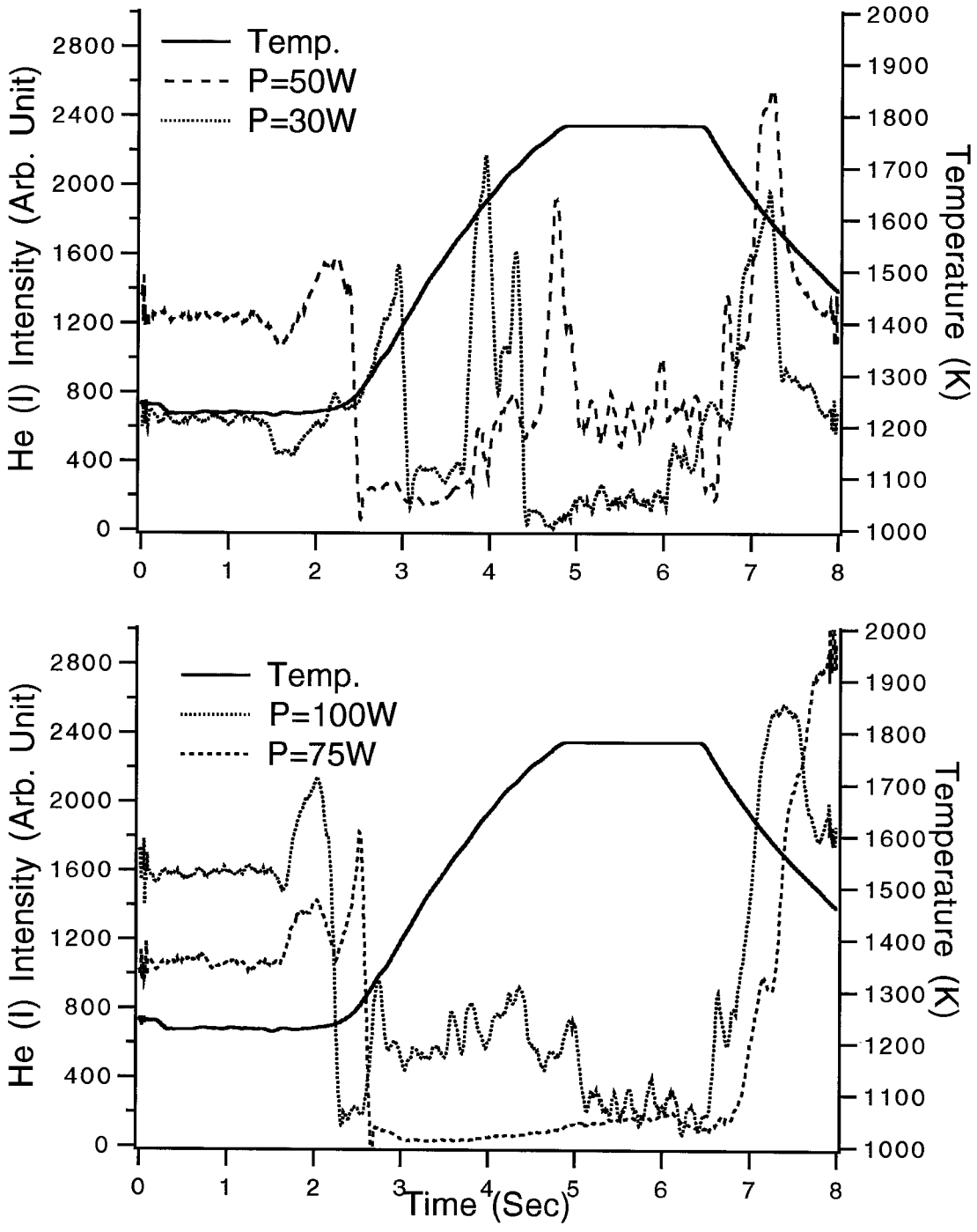

Figure 3.3. **Temporal emission behavior for He (I) line at rf power of 30, 50, 75 and 100 W and time-temperature profile for furnace wall .**

The dramatic decrease of He (I) line emission could be the result of plasma shut-off, which might arise because of changes of power coupling efficiency between the load impedance and output impedance of the rf oscillator. This impedance matching might have been altered by the thermionic electrons emitted from graphite surface [51] at high temperature. At atmospheric pressure, the mean free path for electrons in helium is in the μm region [52]. Thermionic electrons originating from the surface of the center electrode are likely to have a greater effect on plasma processes than those generated some distance away at the furnace wall where the field is less intense. It is generally accepted that there are two populations of electrons in plasma with different temperature [53, 54]. A high temperature group promotes excitation and ionization whereas a lower temperature, higher density fraction is involved in collisional de-excitation processes. Thermionic emission from the furnace wall may serve to flood the plasma with a large number of low-energy electrons, thereby altering the impedance matching.

This observation of He (I) line is comparable with the observation of Falk et al. [53] for FANES source. Falk and his co-workers reported the characteristics of the discharge voltage as a function of the cathode temperature , where the furnace acts as the cathode, for different current intensity and 9 hPa helium gas pressure which is depicted in Figure 3.4 . As seen in the figure the discharge voltage drops dramatically at around 1700 K.

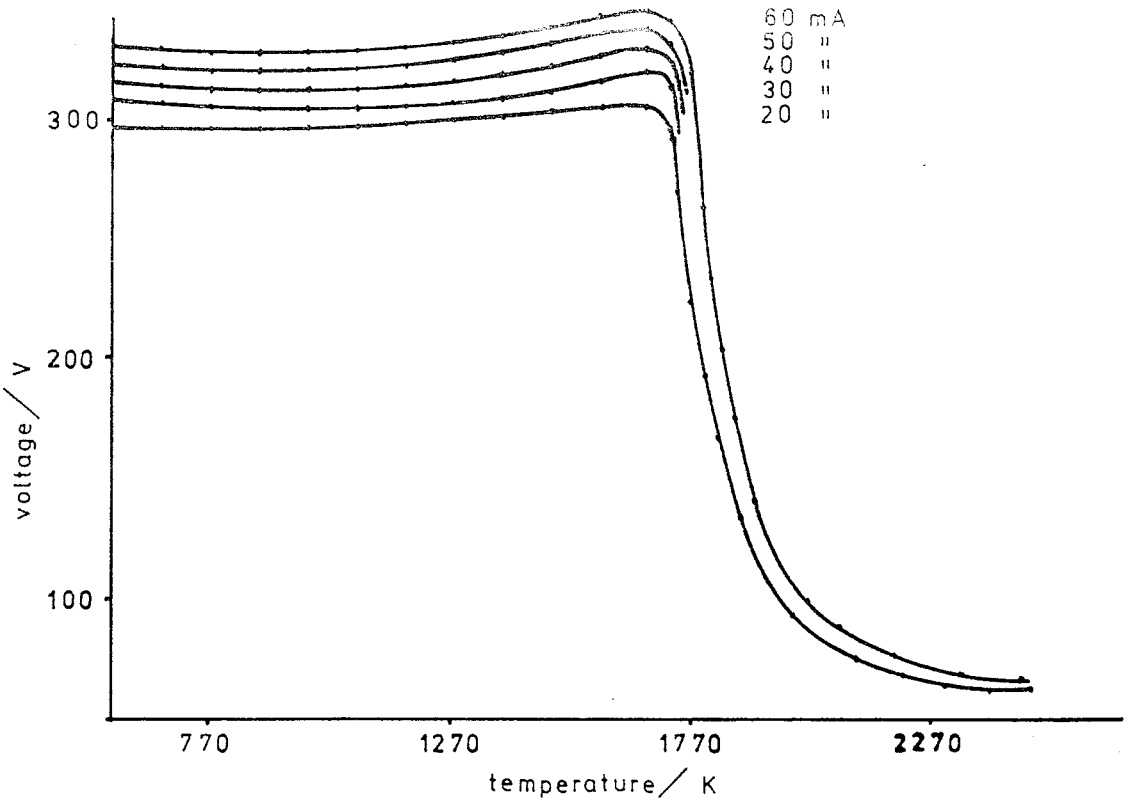

Figure 3.4. Discharge voltage as a function of the cathode temperature for helium at 9 hPa. (Adapted from H. Falk *et al.,* Prog. Analyt. Spectros., 417,11 (1988), with permission of Pergamon Journal Inc.)

In the same report they also showed the He (318.774 nm) line intensity as a function of cathode temperatures with various applied gas pressure. According to their observation , with rising cathode temperature the intensity at first increases and then decreases drastically at around 1700 K (for 9 hPa discharge pressure) with the emission of electrons from the cathode surface which is depicted in Figure 3.5 as well.

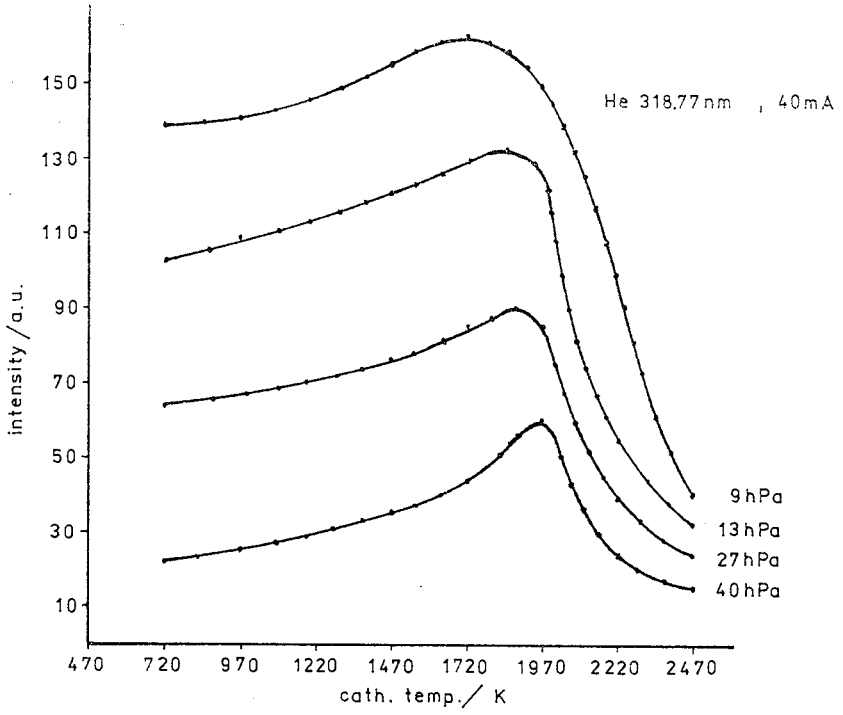

Figure 3.5 : Intensity of the He 318.774 nm line as a function of the cathode temperature at a discharge current intensity for 40 mA and pressure of 9, 13, 27, 40 hPa. (Adapted from H. Falk *et al.,* Prog. Analyt. Spectros., 417, 11 (1988), with permission of Pergamon Journal Inc.)

3.4.3 Reflected Power

Reflected power is an important variable because of the fact that changes in reflected power suggest changes in the amount of power coupled to the plasma and hence changes in the characteristics of plasma. In FAPES, the graphite furnace heats up during the atomization step, and the plasma

impedance changes as a result of the evolution of thermionic electrons from the hot graphite surfaces. This change in the plasma impedance necessitates the use of an impedance matching network to maintain the reflected power at a minimum and to protect the rf power supply.

The change of reflected power during the atomization step due to furnace wall temperature was studied at rf power of 30, 50, 75 and 100 W at 13.56 MHz. Four replicate measurements were carried out for each determination which were then averaged and presented on the Figure. Measurements of the plasma reflected power levels were obtained from the appropriate I/O port on the rear of the RFX-600 rf power supply (Advanced Energy, Fort Collins, CO, USA). This 0-5 V signal was directly compatible with the data acquisition system. The furnace wall temperature was also measured simultaneously.

The results of this experiments are given in Figure 3.6. Initially there is no significant change in reflected power, but at a higher furnace wall temperature, the reflected power increases sharply for 50, 75 and 100 W plasma power. For 30 W plasma power, the increase in reflected power is gradual starting at around a furnace wall temperature of 1450 K , however, a sharp increase in reflected power happens at around 1550 K, 1650 K and 1700 K of the furnace wall temperature for the plasma power of 100, 75 and 50 W respectively. The reflected power level rises to about 88, 65, 40 and 20 W for the forward power of 100, 75, 50 and 30 W respectively.

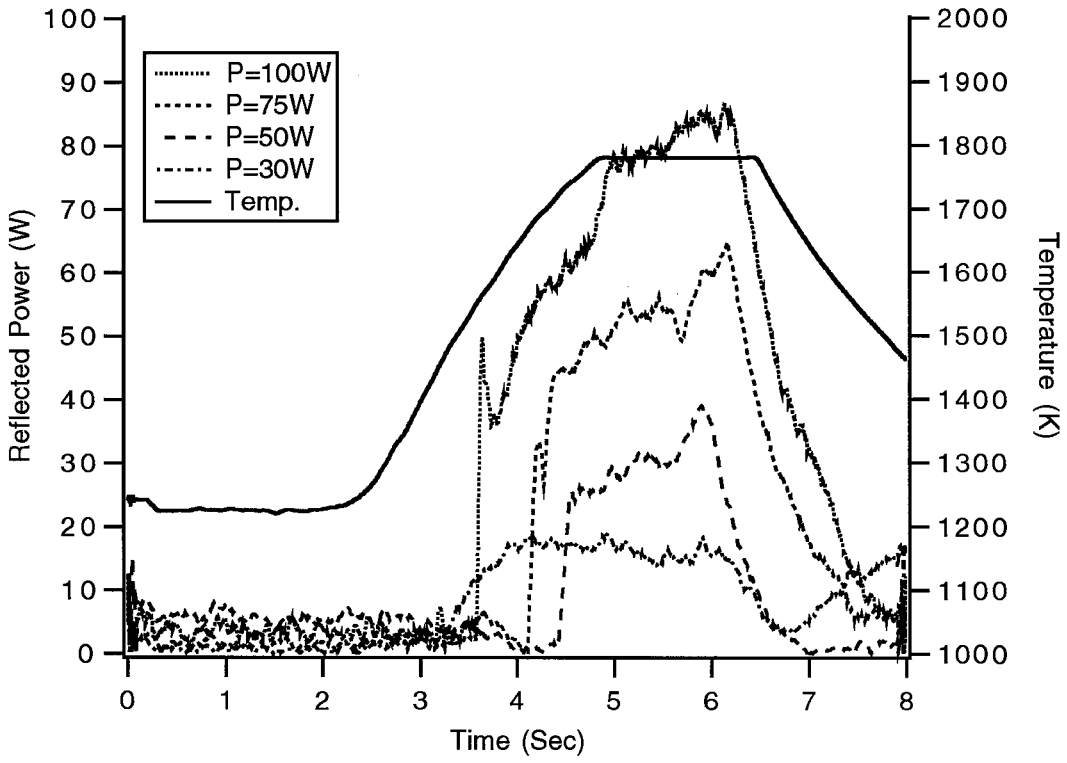

Figure 3.6: Temporal behavior for reflected power at rf powers of 30 , 50, 75 and 100 W along with time-temperature profile for furnace wall.

The change in reflected power level is apparently determined by the temperature. It is also evident from this figure, however, it is not the absolute temperature of the furnace wall that accounts for the time dependence of the reflected power level. This is clear from the nature of reflected power where the

change of reflected power does not follow the changing pattern of the change of furnace wall temperature . Thus, it appears that it is the temperature of the center rf electrode that influences the magnitude of the reflected power level, the latter being heated by radiation from the furnace wall. The reason for a rise in reflected power and, hence, a decrease in the efficiency of the coupling of the rf energy into the system is not yet clear. At high temperature, however, thermionic emission of electrons from the graphite surface occurs [51] which might be responsible for the alteration of the impedance matching and, hence, causes a rise in reflected power.

3.5. SUMMARY

Stability of the helium plasma at 13.56 MHz was studied for the FAPES source by examining the He (I) and CO^+ emission lines as well as the reflected power at different rf power. A calculation is also carried out using the Richardson equation to determine the thermionic electron flux for graphite and tungsten. The thermionic electron flux increases exponentially with furnace wall temperature .

Initially, the CO^+ emission intensity increases with rf power and with furnace wall temperature followed by a dramatic decrease at around 1450 K . The evolution of thermionic electrons might be responsible for the depression of CO^+ emission intensity by recombining with CO^+ or with He_2^+, and, hence changing in the excitation characteristics for CO^+.

A time - resolved study of the He (I) emission line showed complex emission characteristics during the atomization step. Like CO^+, the emission intensity for He (I) also shows an initial increase with rf power and with furnace wall temperature which is followed by a sudden decrease with increasing furnace wall temperature. This sudden decrease happens earlier for higher rf powers than for lower ones . This dramatic decrease is indicative of the plasma shut-off at higher temperature as a result of the changing of power coupling efficiency between the load impedance and output impedance of the rf oscillator .

Reflected power also shows a significant change at higher temperature . The reflected power level rises at about 88, 65, 40 and 20 W for the forward power of 100, 75, 50 and 30 W respectively. The magnitude of the reflected power level does not depends absolutely on the furnace wall temperature but on the center rf electrode which being heated from the furnace wall by radiation. It is suggested that thermionic emission of electrons from the graphite surface might be responsible for the alteration of the impedance matching and, hence, cause an increase in reflected power.

CHAPTER 4

TEMPORAL AND SPATIAL EMISSION AND TEMPORAL ABSORPTION CHARACTERISTICS OF SILVER IN FAPES

4.1 INTRODUCTION

For GFAAS, the temporal response of the analyte absorption is an important diagnostic tool and has often been combined with kinetic and thermodynamic calculations in order to determine the analyte atomization mechanisms during the high temperature atomization step [55-58]. The temporal response of the analyte signal is also an important factor that affects the analytical characteristics; for example, sensitivity, detection limit, precision, and linear range as well as the matrix effects for analytical determinations by GFAAS [28, 59]. For FAPES, the temporal response of the analyte signal is likely to be different from that in GFAAS mainly because of two factors. Firstly, for FAPES, the presence of the electrode and plasma inside the graphite furnace may cause a difference in the atomization characteristics from those in GFAAS. The presence of the plasma may affect atom formation processes by participating in the equilibria for condensed and gas phase species. Gas phase concentrations of different species, which influence the atomization characteristics of analytes , may be different due to the presence of plasma, compared with those where plasma is absent. Secondly, due to the presence of the rf electrode inside the furnace, the vaporization characteristics of analytes in FAPES may be different from those in GFAAS.

The rf electrode can act as a second surface where analytes can condense and then vaporize to form a second peak. Smith et al. reported double peaks for Ag at high analyte amounts and low rf powers and speculated that the appearance of double peaks was due to the atomization characteristics of Ag in FAPES [24]. Hettipathirana *et al.* reported double peak for ETAAS absorption for Ag when an rf electrode was present inside the furnace and suggested that without a plasma, the electrode acts as a condensation site for atoms and/or oxides which are subsequently re-atomized at higher furnace temperatures as the electrode is heated radiatively and by convection [60] . Sturgeon *et al.* reported the appearance of double peaks for Cd at low rf powers in FAPES [23]. In addition, for Cd, Cu, Ni and Be, an early shift in the position of peak maximum was observed whereas for Fe, Pb, P and Bi, no shift were observed with increasing rf power up to 75 W [48]. Sturgeon *et al.* suggested that the observed shifts were due to increased plasma volume and density which occur with increasing rf power; electron collision causing more efficient excitation; possible changes in the actual observation zone; and reduction of self-absorption in the larger, hotter plasma [48]. Hettipathirana *et al.* reported an increase in peak width and peak area and decrease the appearance temperature for Ag with increasing plasma power from 14 W to 38 W [65]. In addition , for lead a decrease in appearance temperature and presence of a second peak were observed with increasing plasma power up to 40 W [60]. In the same report, the authors also mentioned an increase in the peak intensity and the presence of a second peak for manganese when the plasma power was increased up to 40 W . For HA-FANES, Riby at. el. reported two unresolved peaks for Cr, and suggested that Cr condensation on the electrode was the origin of these two peaks [61].

In an effort to understand more fully the influence of plasma power on the response of analyte signal in FAPES, a study of spatially resolved atomic emission followed by a time resolved atomic absorption and atomic emission was undertaken. This chapter presents the results of this study for Ag. Spatial distribution of the atomic emission signal and the effects of plasma on analyte atomization and vaporization characteristics are discussed. In addition, the effects of the plasma excitation process on the temporal response of analyte signal during the analyte vaporization and atomization are presented .

4.2 EXPERIMENTAL

For a complete description of the experimental set-up the reader is referred to chapter two of this thesis. This experimental system and an off-axis mount , usually known as vertical-mount , for the rf electrode were employed. For the results presented in this chapter, four replicate measurements were averaged and subjected to a 25-point Savitzky-Golay smoothing procedure [62]. Analytical parameters, such as absorbance, peak area, and peak width , were calculated for each sample deposition. The analyte appearance temperatures were calculated on the basis of their appearance time and temperature-time profile of the graphite furnace. The appearance time was defined as the time taken to reach the average base line plus three standard deviations of the base line noise for the emission or the absorption signal. The peak temperature was defined as the temperature at which the maximum emission or absorption occurs. Prior to analyses all analyte solutions in 1% (v/v) HNO_3 were prepared

from 1000 mg L^{-1} stock solution by serial dilution . Silver stock solution was prepared by dissolving analytical grade $AgNO_3$ (BDH, Toronto, Canada). Nitric acid solutions were prepared by using the analytical grade reagent (BDH, Toronto, Canada).

On the inside wall of the furnace a 10 μL aliquot of analyte solution was deposited by using an Eppendorf 0.5 - 10 μL micro pipette. Helium (Union Carbide, Toronto, Canada) was used to purge the plasma source work-head. The furnace temperature was set to 500 K for 40 second to ash the sample. This time was sufficient to exclude water vapor from inside the plasma source work-head before the ignition of plasma. After the ashing, there was 10 second lag before the plasma was ignited. The lag time was followed by the ramping of the furnace temperature to 2200 K in 5 second for all determinations. For each determination four replicate measurements were carried out. The blank determinations were carried out by depositing the same amount of 1% (v/v) HNO_3 solution. All determinations were carried out by using the atomic resonance line of Ag (at 328.07 nm).

4.3 RESULTS AND DISCUSSION

4.3.1. Spatial Effect of Plasma on Analyte Emission

The spatial distribution of the atomic emission signal was studied by depositing the analyte sample on the furnace wall and the temporal response at different radial positions from the furnace was recorded. The results of this experiment,

when 3 ng of Ag is deposited on the furnace wall and the plasma was run at 30 W power, are given in Figure 4.1.

When the center of the furnace is focused on the monochromator entrance slit , two peaks are observed. The first one is very sharp with an appearance temperature of 1240 K and a peak temperature of 1275 K. The second peak has an apparent peak temperature of 1460 K. At the position of 0.25 mm and 0.75 mm from the furnace center, two distinct peaks for each position are also observed . For both positions the appearance and peak temperature for the first peak are similar to the center position whereas for the second peak the apparent peak temperature is 1455 K and 1495 K for 0.25 mm and 0.75 mm respectively. The first peak tends to merge into the second one when the monochromator is set to observe at 1.25 mm from the center having the appearance temperature of 1250 K and peak temperature for the first one is 1325 K and the apparent temperature for the second peak is 1440 K. The first peak appears again having the same appearance temperature, 1240 K, and the peak temperature of 1250 K, 1275 K and 1275 K for the position of 1.75 mm, 2.25 mm and 2.75 mm from the center respectively.

These observations suggest that the rf electrode acts as a condensation site for species vaporized from the surface wall with subsequent "second surface" vaporization and excitation. The decrease in the size of the initial peak with distance from the center shows that the condensation rate decreases with increasing distance from the center. This decrease also might be because of excitation efficiency changes with the distance from the center electrode. The

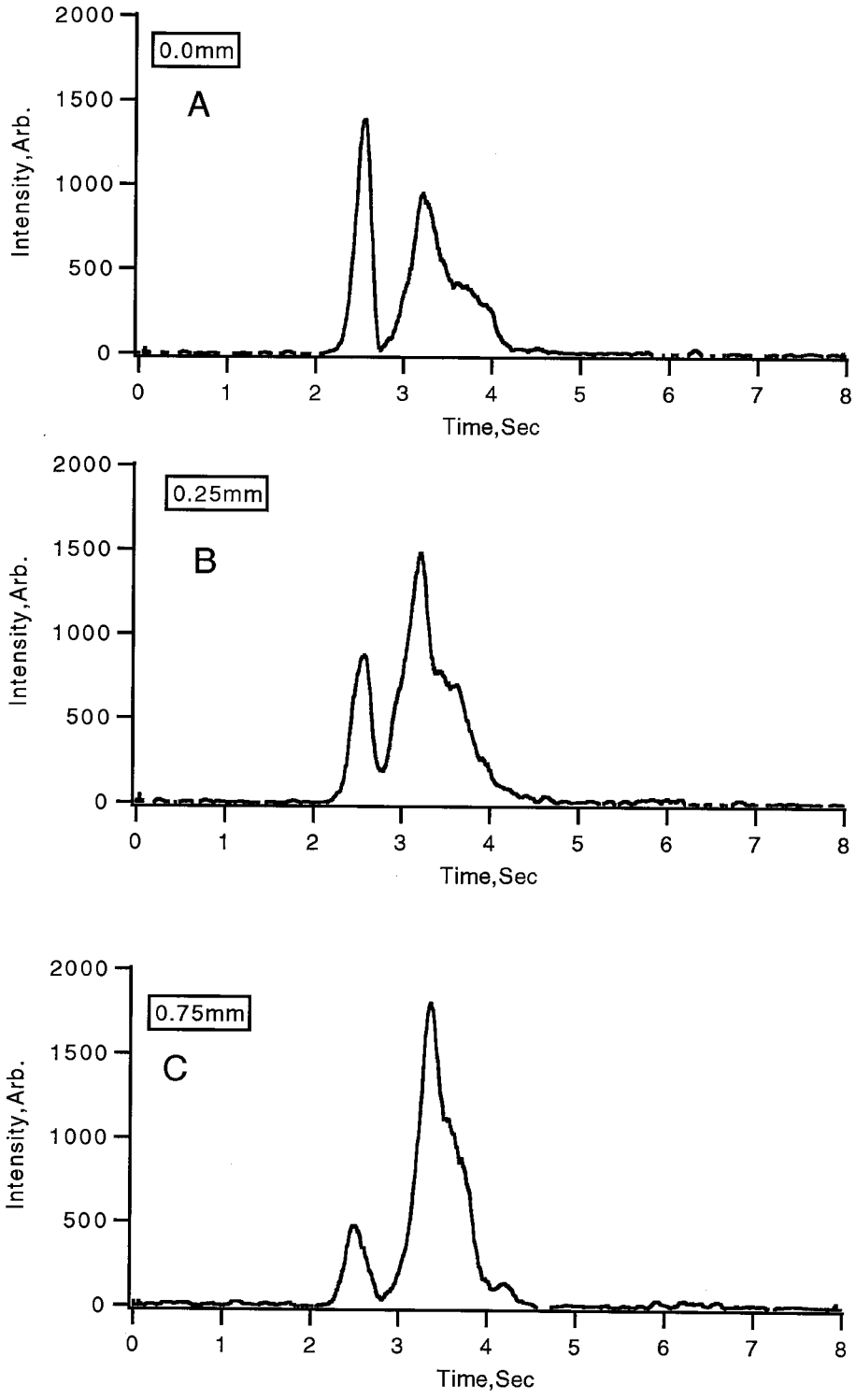

Figure 4.1.A, 4.1.B and 4.1.C **(continued on page 62)**

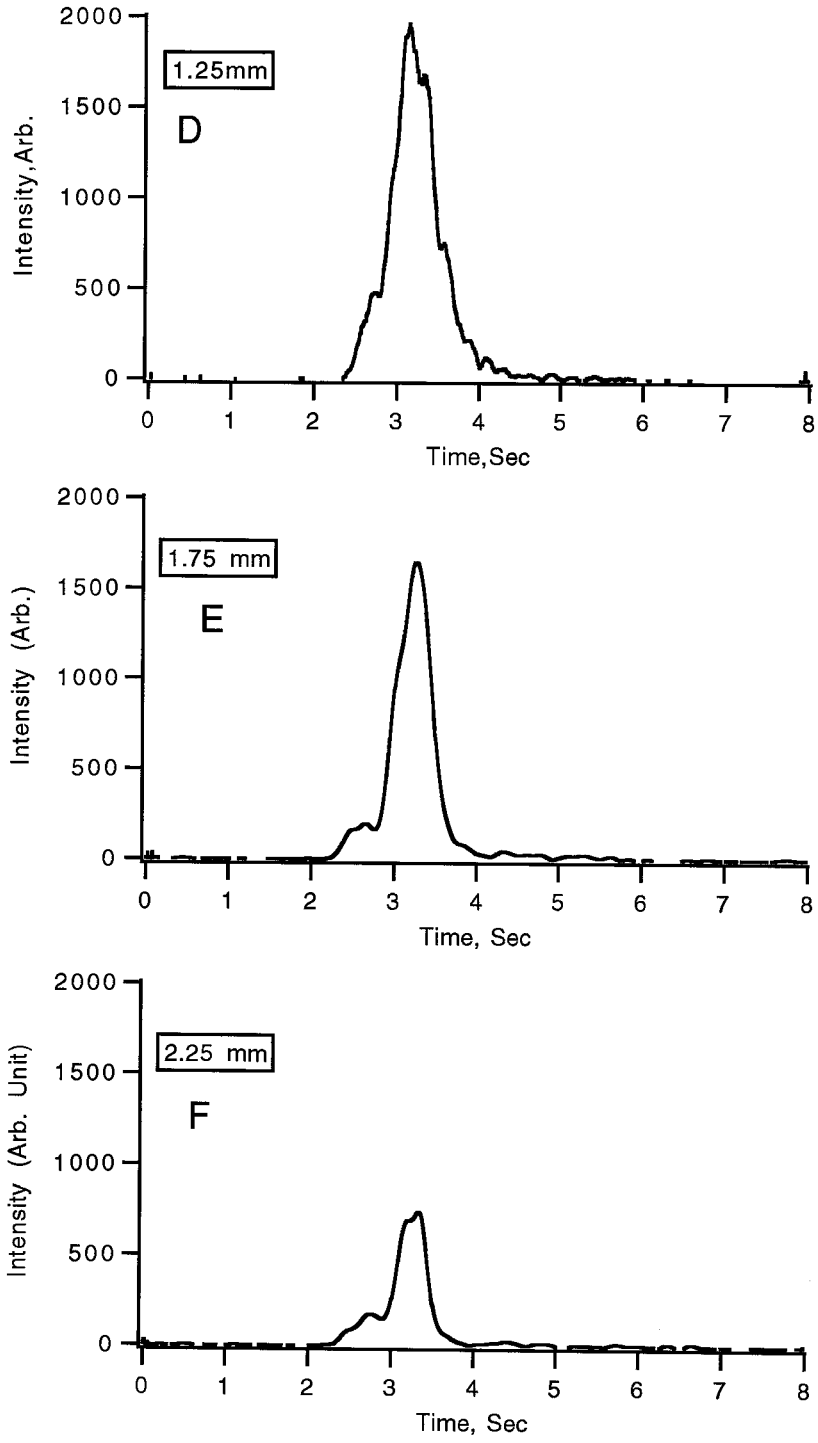

Figure 4.1.D, 4.1.E and 4.1.F **(continued on page 63)**

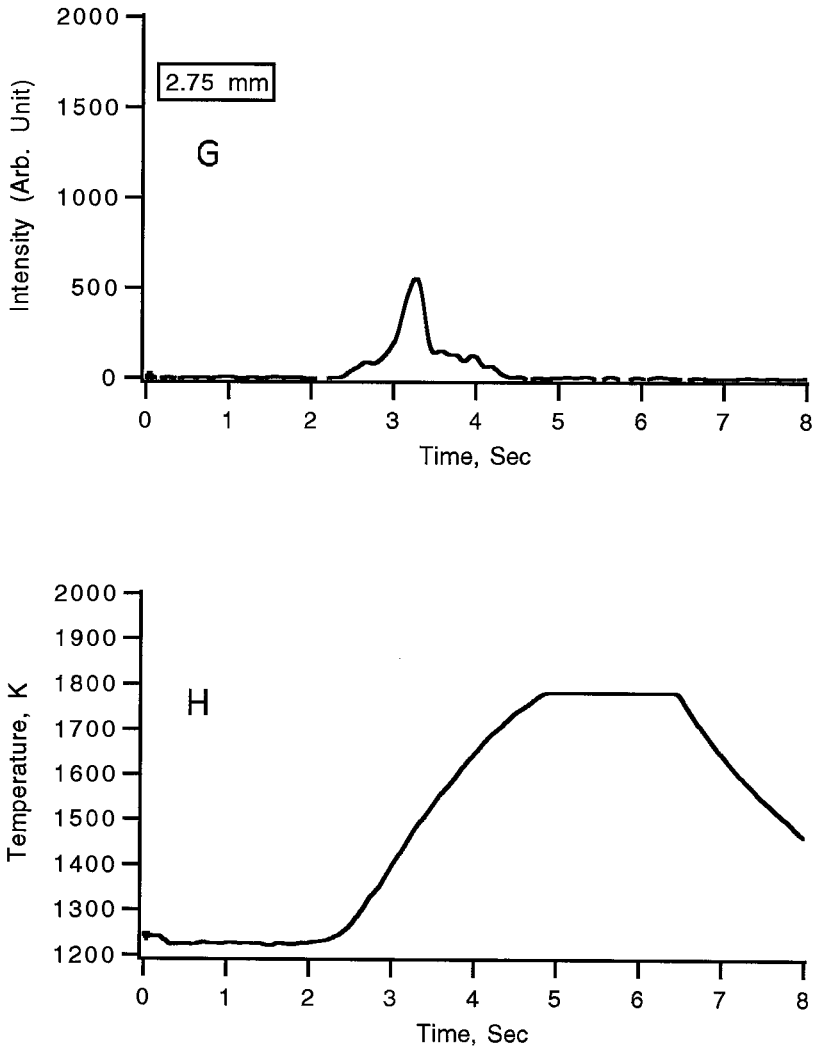

Figure 4.1. **Temporal response of the Ag emission signal at an rf power of 30 W for 3 ng of Ag deposited on the furnace wall when the monochromator is focused at 0.0 mm (A), 0.25 mm (B), 0.75 mm (C), 1.25 mm (D), 1.75 mm (E), 2.25 mm (F) and 2.75 mm (G) with respect to the furnace center ; and the Temperature-Time profile for the furnace wall (H).**

delay in the onset of the second peak is the result of delaying heating of the rf electrode relative to the furnace wall is somewhat similar to the situation encountered during the radiant heating of the L'vov platform.

The process of condensation on the cooler inside surface of the furnace is consistent with recent studies for GFAAS [63, 64] and for FAPES [60]. L'vov *et al.* observed double peaks when a platform is present inside the furnace [63]. To condense the analyte followed by the re-vaporization in the atomization step to achieve the temporal isothermality, Hocquellet used a "second-surface trap" inside the furnace [64]. Hettipathirana *et al.* observed double peaks for Ag atomic absorption when the sample was deposited on the furnace wall in the presence of a co-axial rod in the FAPES system [60].

Figure 4.2 provides the spatial distribution of analyte signal in the graphite furnace at an rf power of 30 W for 3 ng of Ag deposited on the furnace wall. Both peak height (Figure 4.2. A) and peak area (Figure 4.2. B) show that the signal intensity increases with increasing distance from the furnace center and reaches maximum at 1.25 mm from the center . This spatial distribution was observed by translating an image of the FAPES source laterally in increments of 0.50 mm.

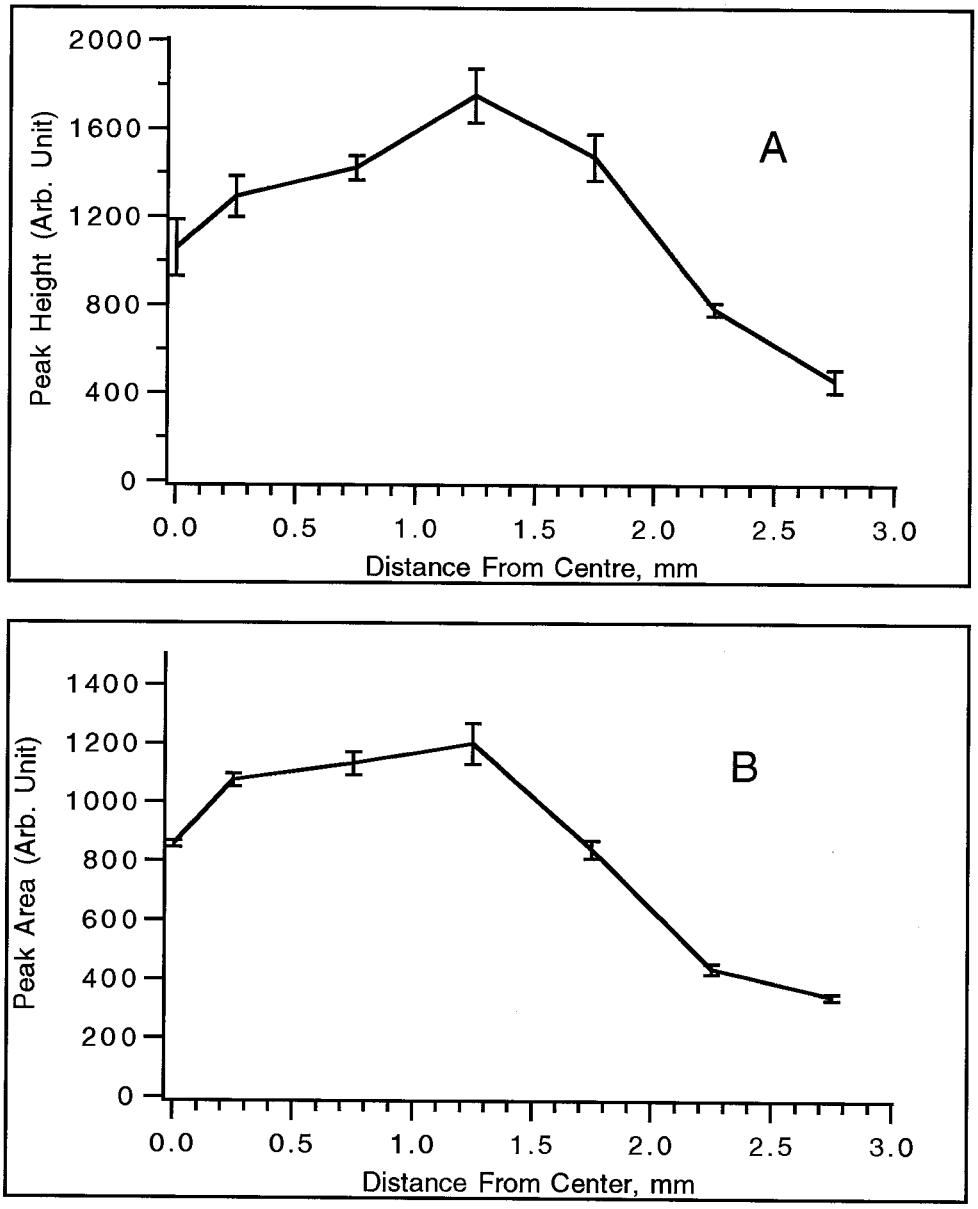

Figure 4.2. Spatial response of the Ag emission at an rf power of 30 W for 3 ng of Ag deposited on the furnace wall. A : Peak Height Vs radial distance, B : Peak Area Vs radial distance.

4.3.2. Effect of Plasma Power on analyte Emission and Absorption

The effect of rf power on the emission signal was studied for 1 ng of Ag deposited on the furnace wall while the center of the furnace is focused on the monochromator entrance slit. The results are provided in Figure 4.3. As seen in the figure, the emission signal is shifted to earlier time by 248 ms when the rf power is increased from 30 W to 150 W. The tendency of showing double peaks also disappears when the rf power is increased to 125 W .

The observed shift of the emission signal with increasing rf power may be due to an increased evaporation rate of Ag from the furnace wall when the plasma is present [65]. It is also might be because of some plasma-assisted heating of the surface of the furnace wall at higher plasma powers. At higher plasma power, for example 125 W and higher, the rf electrode could become too hot to act as a second surface for condensation and as a result, the second peak was not observed.

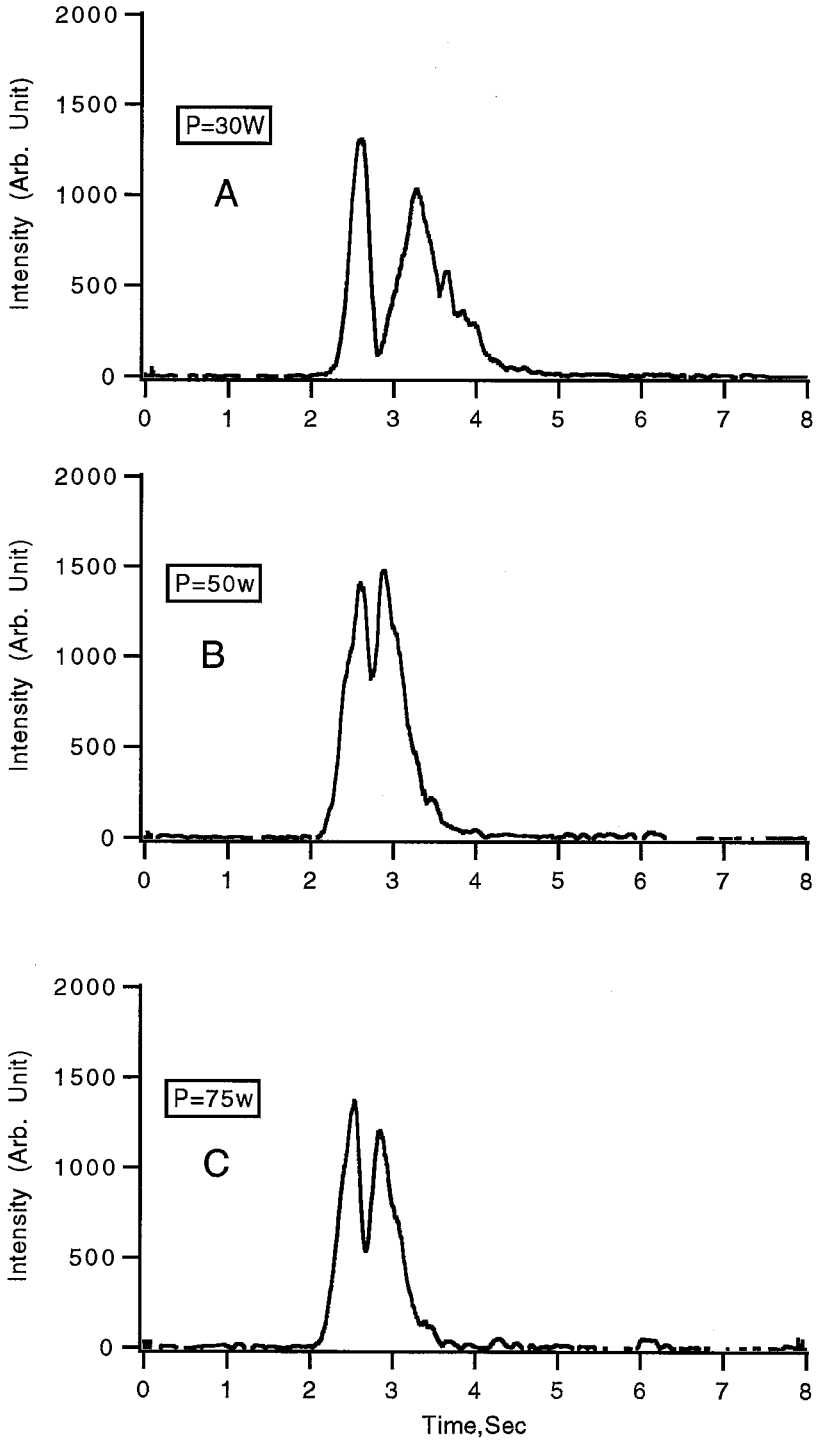

Figure 4.3.A , 4.3.B and 4.3.C **(Continued on page 68)**

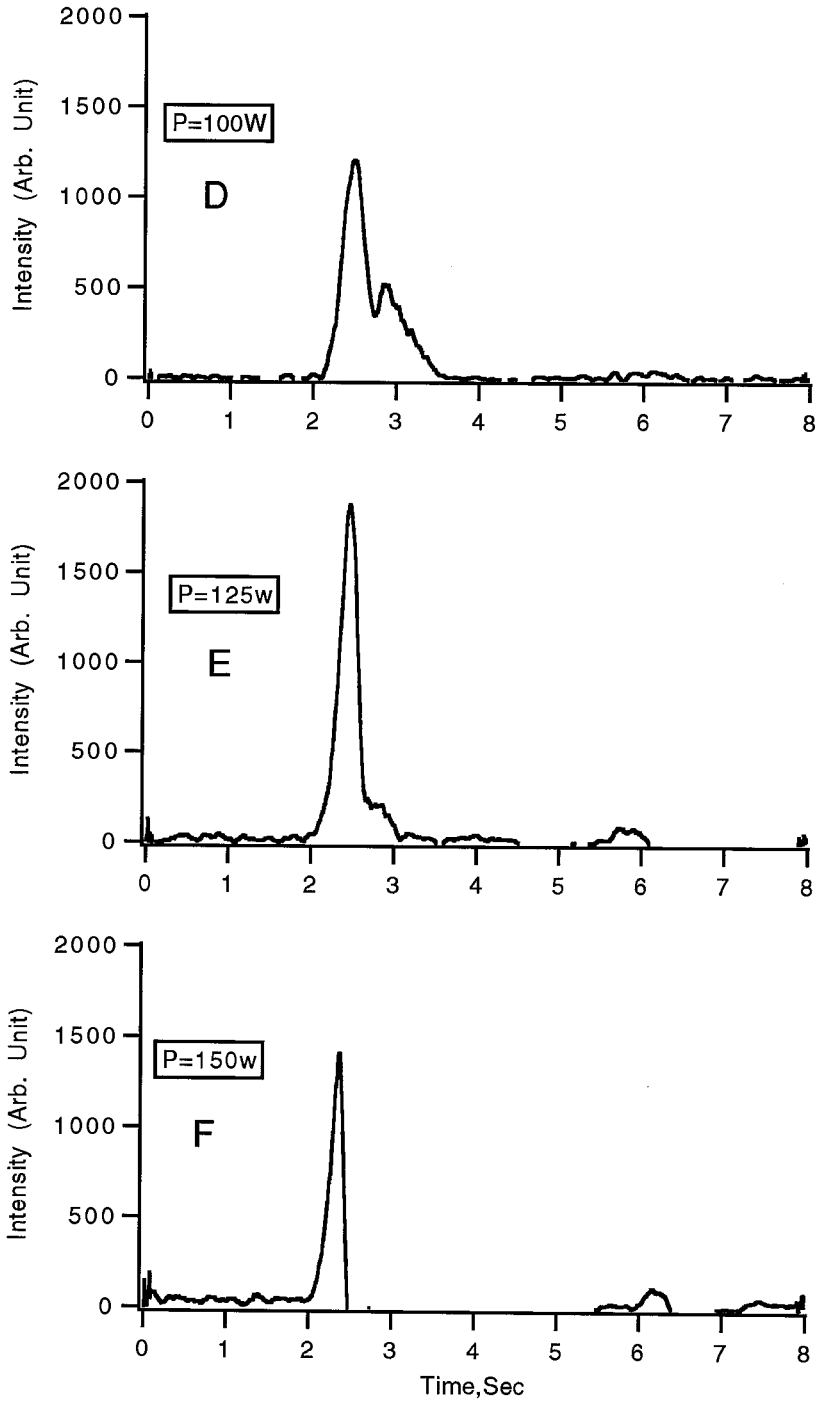

Figure 4.3. Temporal response of the Ag atomic emission signal for 1 ng of Ag deposited on the furnace wall at an rf power of 30 (A), 50 (B), 75 (C), 100 (D), 125 (E) and 150 (F) W.

As seen in Figure 4.3 , for plasma power 30, 50, 75 and 100 W the emission signal changes gradually; but when the plasma power is raised to 125 W, the change in emission signal is dramatic. The changes in peak area for emission signal at different plasma power is shown in Figure 4.4.

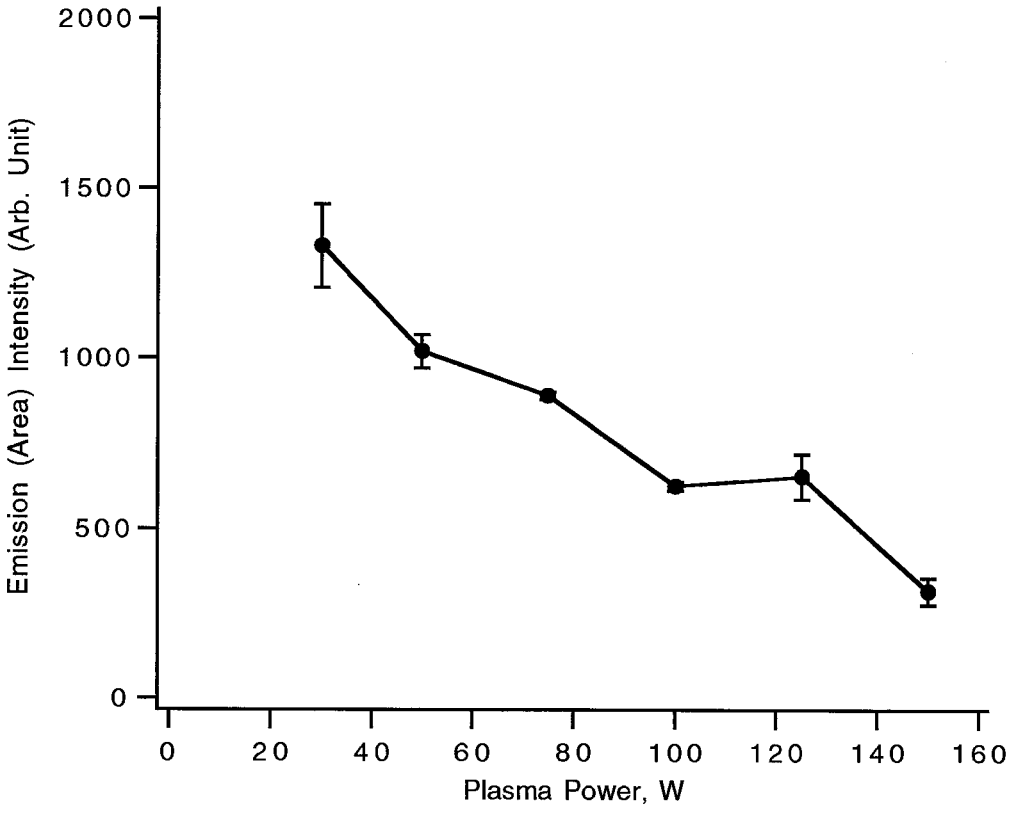

Figure 4.4: Effect of plasma power on emission signal for 1 ng of Ag deposited on the furnace wall at an rf power of 30, 50, 75, 100, 125 and 150 W.

With increasing rf power there might be some loss of analyte due to pre-atomization loss, changes in the excitation characteristics , or an increase in ionization of Ag. The drastic decrease in the analyte signal at the rf power of 125 W and more is likely because of plasma extinguishes which is consistent with the observation of He (I) line emission at different plasma power (Section 3.4.2).

Pre-atomization losses in graphite furnace methods are due to the high volatility of the analyte molecular species and a slow heating rate of the graphite furnace coupled with a lower atomization temperature. The atomization losses may also be significant because of an increase in diffusion with increasing temperature at high plasma powers. The analyte loss may also be due to rf sputtering from the furnace wall prior to atomization . However, Sturgeon *et al.* reported no measurable decrease in the Ag emission signal even during an extended 2 minute period of plasma operation prior to atomization step [54].

The excitation characteristics of analyte could be affected by the presence of thermionic electrons at high plasma powers . The excitation characteristics can be affected by decreased collisional excitation rate (due to changes in the electron number density) and/or by increased collisional de-excitation rate (due to low energy thermionic electrons). Although no changes in the reflected power are observed before 3.5 s (up to 100 W plasma) into the atomization step , some temporal characteristics of ionic species such as CO^+ is attributed to the evolution of thermionic electrons. The study of CO^+ emission behavior as

a function of rf power shows that CO^+ intensity decreases drastically at around 1450 K of the furnace temperature (Section 3.4.1) and it is suggested that thermionic electrons might recombine with CO^+ and responsible for the depression of CO^+ emission intensity. Furthermore, the He-excitation temperature measurement for FAPES by Sturgeon *at el.* [50] and Ar and He-excitation temperature measurement for HC-FANES by Falk *et al.* [53] show that the thermionic electrons do not affect the excitation temperature at higher furnace temperatures; however, they can influence the electron density of the plasma.

For plasma spectrometric methods, analyte ionization may also be significant. As the plasma power increases, it not only increases analyte excitation, and, hence, increases the emission but also increases analyte ionization. For HC-FANES, Falk *at el.* reported an increase in the emission intensity for Ni , Cr, Cu, Fe , Co and Al when the discharge current is increased from 20 to 60 mA [53]. However , the power coupled to the HC-FANES source is only 18 W at a discharge current of 60 mA. For HA-FANES, Harnly *at el.* reported a constant emission intensity for Cu and Cd above a threshold current (50 and 20 mA for Cu and Cd respectively) when the discharge current was changed from 10 to 80 mA [61]. FANES (with the excitation temperature ranging from 1000 - 3000 K) is considered to be a relatively low ionization plasma source compared with a high temperature plasma source like the ICP (with the excitation temperature ranging from 4000 - 7000 K) [18]. For the rf plasma sources in FAPES, the excitation temperature is ranging from 3000 - 5000 K depending on the rf power and the thermometric species used for the measurement [45]. Hettipathirana *at el.* reported Ag ionization in FAPES at an

rf power of 40 W [60] . They found that the integrated emission intensity for Ag is decreased in the presence of Na interferent compared to that without interferent and suggested that there is an ionization suppression of Ag when Na is present during the atomization. It is most likely that the analyte ionization may be significant at higher rf powers, and, hence, a source for the suppression of atomic emission signal intensity in FAPES.

A study of time resolved atomic absorption and emission were taken under the same conditions at different plasma power to understand the atomic population inside the furnace. The results of this experiment , when 1 ng of Ag was deposited on the furnace wall and the plasma was run at different (0 W, 30 W, 50 W, 75 W, 100 W, 125 W and 150 W) power, are given in Figure 4.5. As seen in Figure 4.5, in the absence of a plasma, two peaks are observed for atomic absorption (Fig. 4.5.A). The appearance temperature for the first small peak is 1243 K and that for the second large one is 1532 K. At higher plasma power (75 W and more) the atomic absorption signal tends to show a single peak instead of double peaks (Fig. 4.5.D, 4.5.E, 4.5.F and 4.5.G). The appearance temperature of this peak is approximately the same as the small peak observed without a plasma. This observed single absorption peak at higher plasma power supports the idea that, with increasing the rf power, the rf electrode becomes too hot to act as a second surface for condensation. Figure 4.5 also shows that the response time for absorption is longer than that for the emission at higher plasma power, for example, 50 W or more. The emission signal ended 400 , 88 , 208 , 296 and 1408 ms earlier than that of absorption for the plasma power of 50 , 75 , 100 , 125 and 150 W respectively.

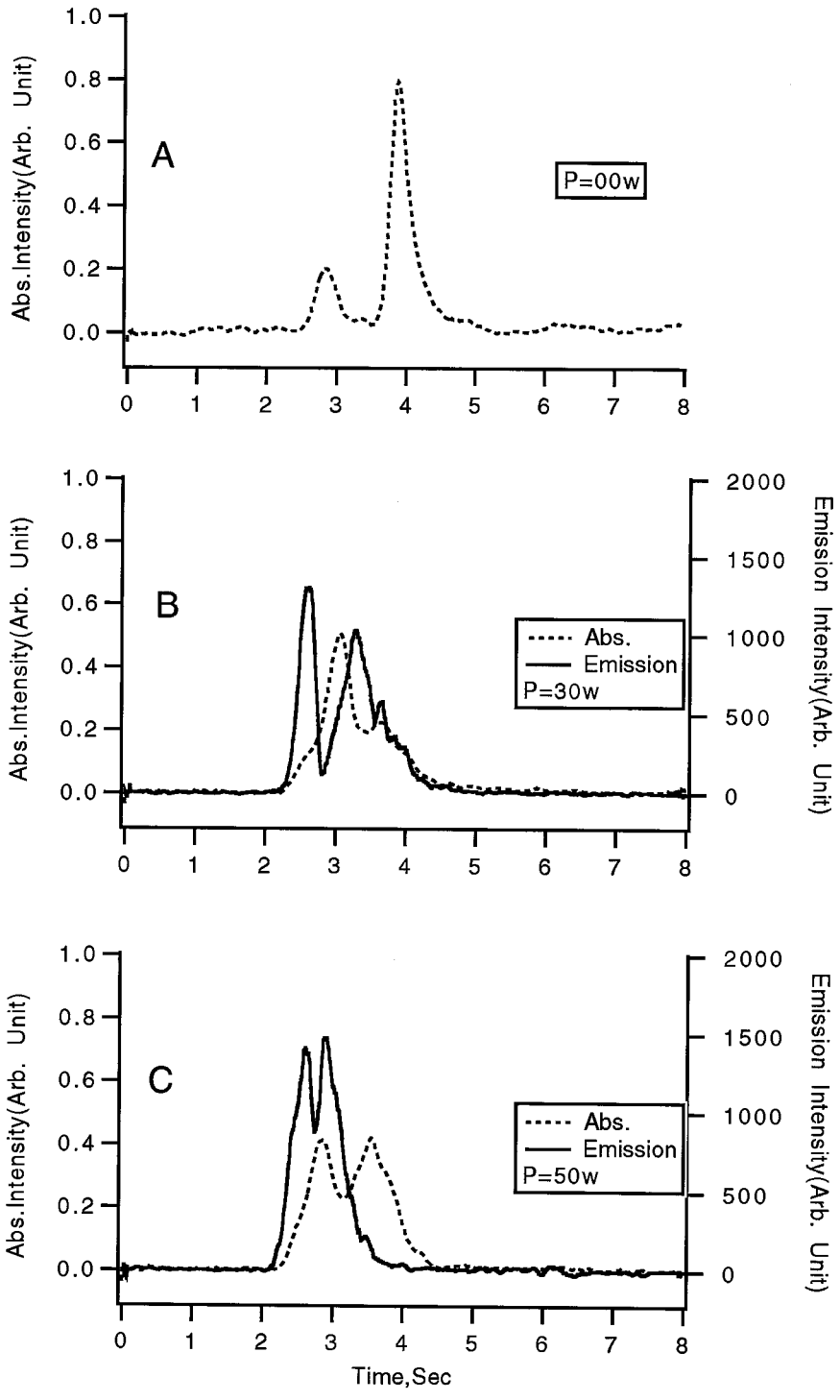

Figure 4.5.A, 4.5.B and 4.5.C **(Continued on Page 74)**

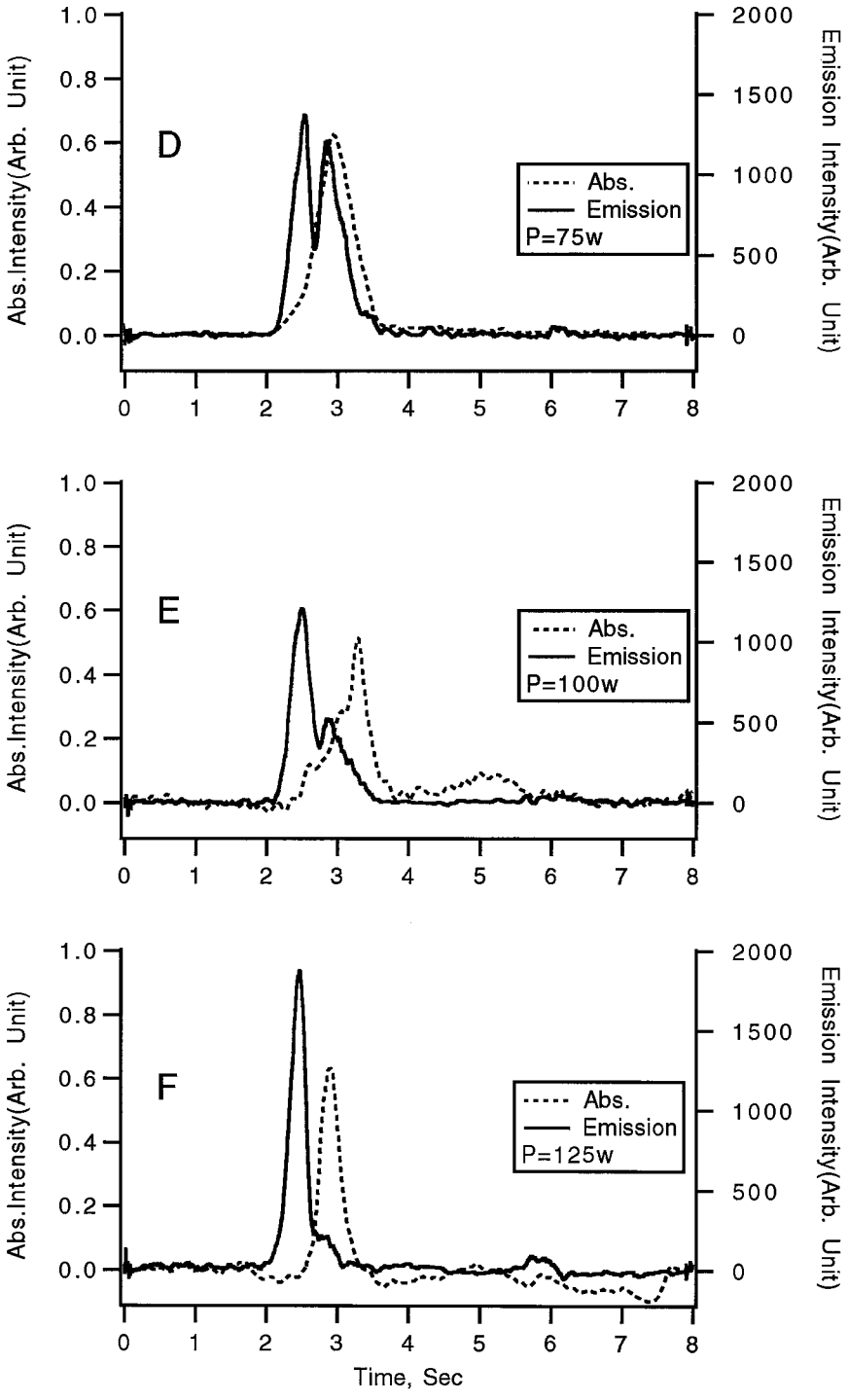

Figure 4.5.D, 4.5.E and 4.5.F (Continued on Page 75)

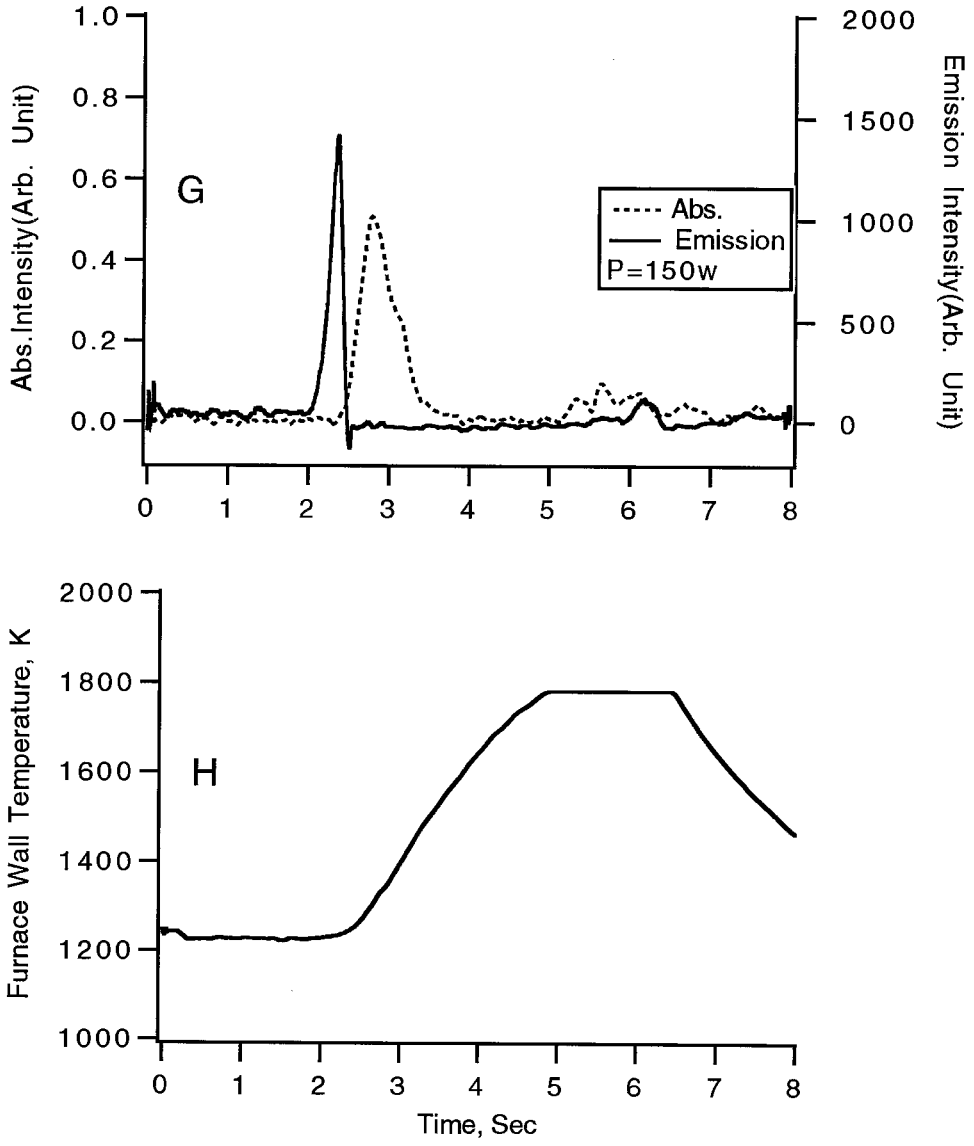

Figure 4.5. Temporal response of the Ag emission and absorption signal at 328.07 nm for 1 ng of Ag deposited on the furnace wall at an rf power of 0 W (A,only absorption), 30 W (B), 50 W (C), 75 W (D), 100 W (E), 125 W (F) and 150 W (G) . The Temperature-Time profile for the furnace wall is also shown on Fig.4.5.H .

This observation suggests that at higher plasma power there are some non-excited atoms present in the system . The only possible reason of not exciting these atoms is the absence of plasma which might be the result of plasma shut-off due to the changes of power coupling efficiency between the load impedance and out put impedance of the rf oscillator (Section 3.4.2) .

Figure 4.6 is a plot of the ratio of absorption and emission as a function of time based on the calculation from Figure 4.5. As seen in the figure, with increasing rf power, the ratio of absorption and emission increases. This increase in absorption-emission ratio indicates that the total fraction of atoms excited from the ground state atoms in the plasma has decreased, during the atomization cycle, with the increase in rf power (except at 75 W plasma). When the system is operated at 30 W plasma power (Fig. 4.6.A) , the rate of non-excited atom is less in comparison of higher plasma power. This calculation again supports the idea that the plasma shuts-off with the increase in operating plasma power.

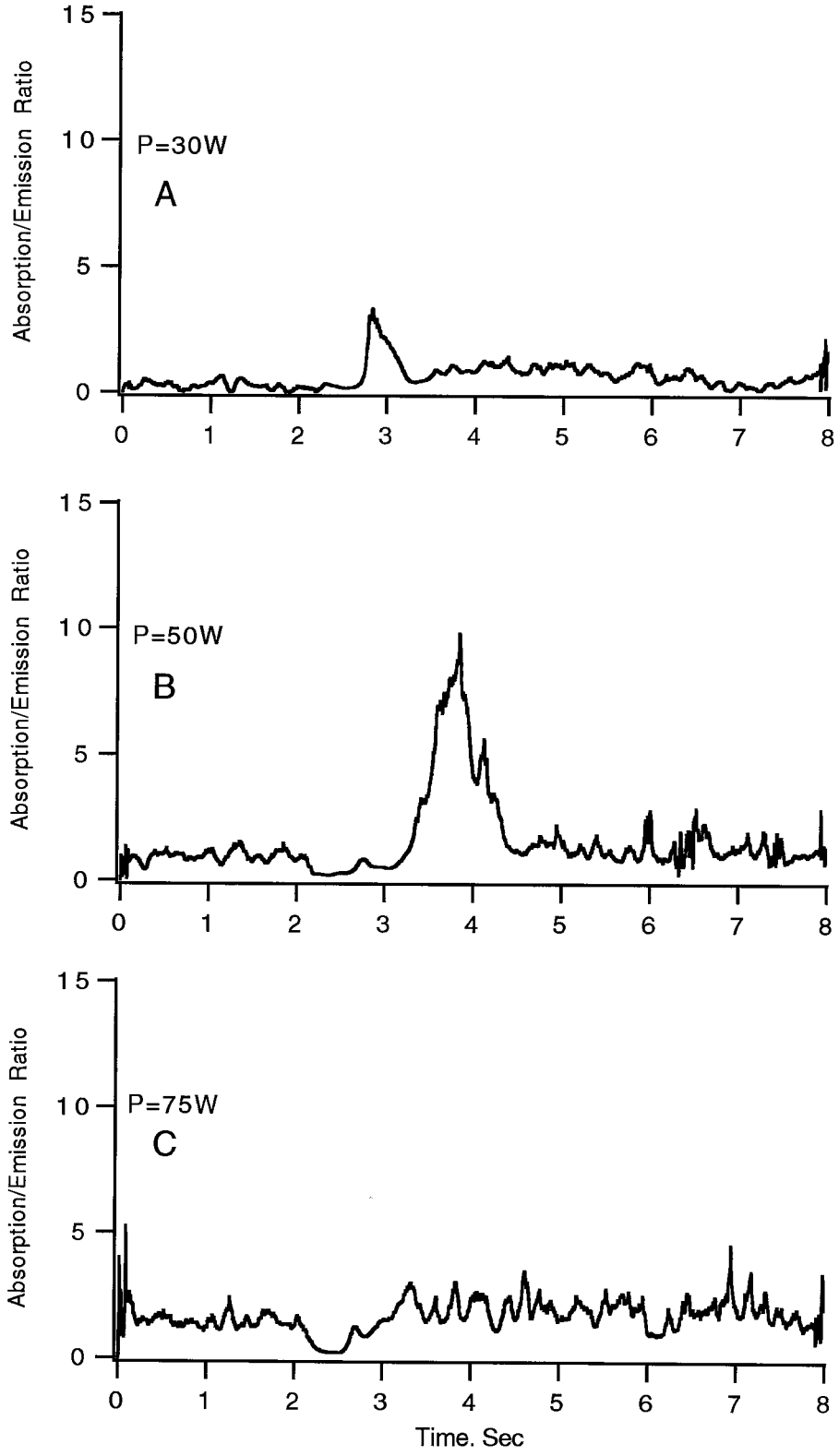

Figure 4.6.A, 4.6.B and 4.6.C **(Continued on Page 78)**

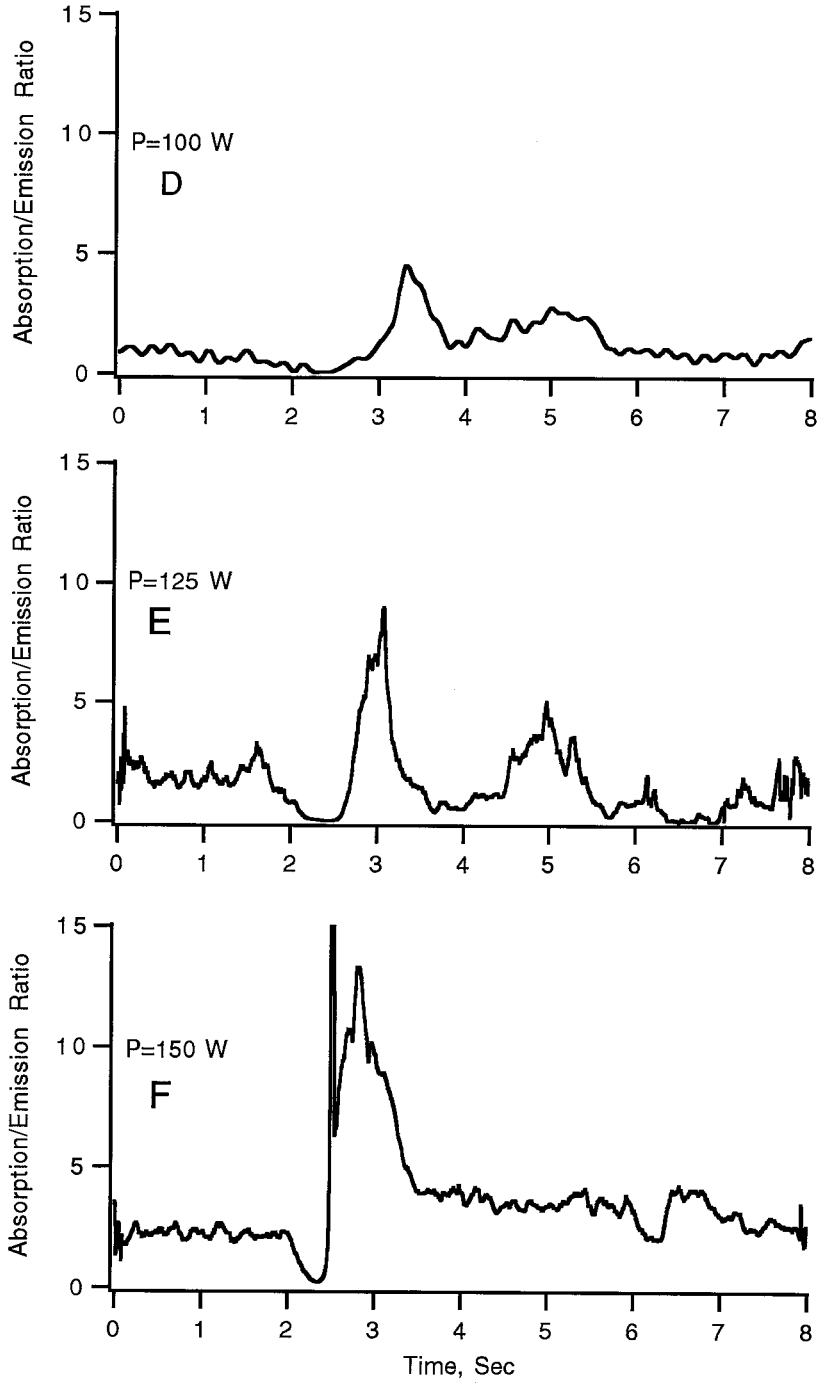

Figure 4.6: Ratio of absorption and emission as a function of time for 1 ng of Ag deposited on the furnace wall at plasma power of 30, 50, 75, 100, 125 and 150 W.

Another important observation is that, not only the emission signal but also the absorption signal shows a decrease in the peak area with increasing plasma power which is presented in Figure 4.7. Unlike emission there is no drastic decrease in analyte absorption signal. The gradual decrease in absorption signal is likely because of the loss of analyte population due to pre-atomization loss or an increase in ionization loss .

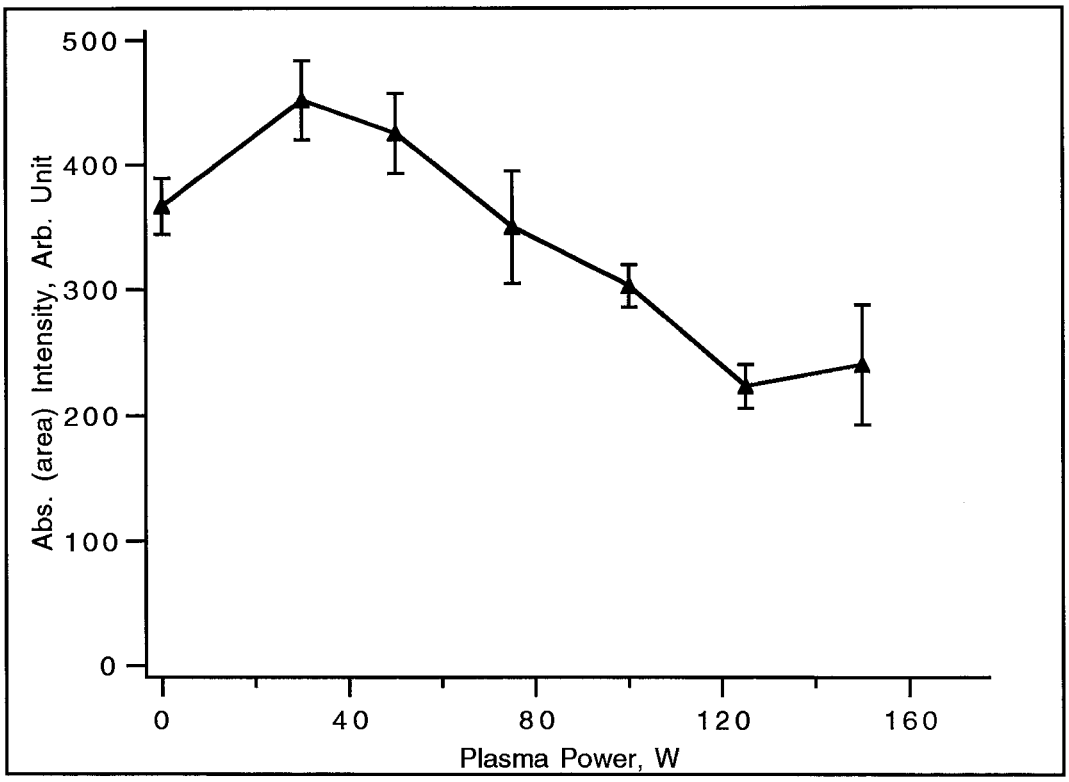

Figure 4.7: Effect of plasma power on absorption signal for 1 ng of Ag deposited on the furnace wall at plasma power of 0, 30, 50, 75, 100, 125 and 150 W.

4.4. SUMMARY

The spatial effect of the plasma on Ag analyte emission was studied for the 328.07 nm Ag resonance line at an rf power of 30 W. The highest emission was observed at 1.25 mm from the center of the furnace. The temporal response of the analyte emission signal in FAPES was also studied for Ag using both atomic absorption and atomic emission spectroscopy while the sample was deposited on the furnace wall.

With lower rf power , the co-axial rod is cooler than the furnace wall resulting a temperature lag between the co-axial rod and the furnace wall . As a result , the co-axial rod acts as a condensation site for atoms and oxides that subsequently vaporize (second - surface vaporization) at higher furnace temperatures. At higher rf power, the co-axial rod becomes hot enough to prevent any condensation, results in the appearance of single peak . The study of rf power effect on analyte also shows a maximum response of Ag emission at 30 W rf power which then decreases with increasing rf power . The absorption signal also decreases with increasing rf power but the rate is much slower than that for emission . This decrease in signal might be because of some loss of analyte population due to pre-atomization loss, changes in the excitation characteristics , or an increase in ionization of Ag. The drastic decrease in the analyte emission signal at the rf power of 125 W and higher is likely because of plasma shut-off.

The calculation of the ratio of absorption and emission shows that there is a portion of atoms that remain un-excited . The amount of un-excited atoms increases with increasing rf power suggesting a plasma shut-off at higher rf power due to the change of power coupling efficiency between the load impedance and output impedance of the rf oscillator.

The emission signal is shifted to earlier time when the rf power is increased from 30 to 150 W by 248 ms, whereas the absorption signal remains virtually the same. This early appearance of Ag emission is likely due to an increased evaporation rate from the furnace wall. The temporal response of both atomic absorption and atomic emission signals shows similar leading and falling edges . These results suggest that the temporal response of Ag in FAPES is determined by the atomization and vaporization characteristics of the analyte rather than by the excitation characteristics .

CHAPTER 5

CONCLUSIONS

The 13.56 MHz helium plasma used for Furnace Atomization Plasma Excitation Spectrometry (FAPES) has been further characterized as a spectrochemical source for elemental analysis. The main objective of this study was to characterize and examine the stability of the radio frequency (rf) helium plasma source, over a wide power range, during the atomization cycle. An effort has been made to more fully understand the influence of higher plasma power, up to 150 W, on the response of analyte signal in FAPES.

One of the persistent spectral features observed for FAPES is emission from CO^+. The temporal response of CO^+ at different radio frequency (rf) power, during the atomization step, shows complex emission characteristics which is likely due to a combination of factors including recombination of ionic species (CO^+ and/or He_2^+) with thermionic electrons and a change in excitation characteristics of the plasma. Initially, the CO^+ intensity increases with increasing the rf power mainly due to the enhanced release of carbon from the rf electrode and furnace wall in the presence of plasma.

Like CO^+ , the temporal response measurements for He (I) line also shows complex emission characteristics during the atomization step. The emission intensity for the He (I) line shows an initial increase with rf power and with furnace wall temperature, followed by a drastic decrease with increasing furnace wall temperature. For higher rf power this drastic decrease happens earlier in time than the lower one. This decrease in emission intensity

indicates the shut-off of plasma at higher temperature as a result of changing of power coupling efficiency between the load impedance and output impedance of the radio frequency oscillator.

The study of reflected power as a function of temperature shows a significant change in reflected power at higher furnace temperature. The reflected power level rises to as much as 88 W for the forward power of 100 W . The magnitude of the reflected power level does not depend absolutely on the furnace wall temperature but on the temperature of center rf electrode which heated from the furnace wall by radiation and by contact with the plasma. Thermionic emission of electrons increases exponentially with furnace wall temperature. The calculated value for the number of electrons per cm^2 of the graphite surface is $3.46x10^6$, $8.43x10^7$ and $1.62x10^9$ for 1300 K, 1400 K and 1500 K of the furnace wall temperature respectively. This large number of thermionic electrons from the graphite surface is likely to be responsible for the alteration of the impedance matching and, hence, causes an increase in reflected power.

The spatial distribution of analyte in the plasma was studied by measuring Ag analyte emission at different radial positions in the furnace at an rf power of 30 W. The result shows an increase in analyte concentration from the center toward the wall, reaching a maximum at 1.25 mm from the center followed by decrease again .The temporal response of the analyte emission signal in FAPES has also been studied for Ag using both atomic absorption and atomic emission spectroscopy while the sample was deposited on the furnace wall . In the presence of plasma, inside the furnace, the rf electrode is heated significantly relative to that without a plasma but no significant change in the

furnace wall temperature is observed. However, during atomization, the temperature of the rf electrode lags relative to that of the furnace wall. This difference in time-temperature characteristics between the graphite furnace and the rf electrode cause condensation of analytes on the rf electrode and subsequent re-vaporization and, as a result, two peaks in the temporal emission profile are observed. The relative intensities and shapes of these two peaks are greatly affected by rf power. Analyte condensation on the rf electrode is severe at lower rf powers but at higher plasma power, for example at 125 W, the rf electrode becomes too hot to act as a second surface for condensation and, as a result , the second peak is not observed.

The effect of the heating rate of the graphite furnace on the temporal response of the emission signals in FAPES is not known yet. The heating rate of a furnace depends mainly on the furnace mass and the rate of initial current supply to the furnace. The effect of heating rate on emission signal could be studied by using furnaces with different mass or by controlling the rate of current supply to the furnace. For this study this was not undertaken mainly due to instrumental limitations and shortage of time. However, it is quite possible that the heating rate of the graphite furnace affects the time-temperature characteristics of the rf electrode relative to the furnace wall, and hence, analyte condensation and re-vaporization characteristics from the rf electrode. Furthermore, results obtained from temporal emission of Ag show an early shift in peak appearance which is likely due to an increased evaporation rate of analyte from the furnace wall . The similarities in peak shapes observed for both atomic emission and absorption signals show that the temporal emission

response in FAPES is determined by atomization and vaporization characteristics of the analyte rather than by excitation characteristics.

An effort has been taken to fully understand the effect of wider rf power on the analyte emission signal for Ag. Results show a decrease in integrated emission intensity at rf powers higher than 30 W . This decrease in emission intensity may be due to pre-atomization loss of analyte, a change in excitation characteristics, and / or an increase in ionization of Ag at higher radio frequency powers. Furthermore, the shape of peaks shows that the residence time for excited Ag atoms is shorter than that for ground state atoms at rf power 50 W and more. This observation suggests that at higher rf powers some of the ground state atoms do not become excited in the system due to quenching of the plasma . The probable reason for plasma extinguishing is a change in power coupling efficiency between the load impedance and output impedance due to rapid change of temperature and/or rapid change in thermionic electron density.

Most of the results described in this thesis show that at higher rf power and higher furnace temperature, thermionic electrons affect the plasma impedance, and the rf power is dissipated by the plasma. The major source of the thermionic electrons are the inner surface of the graphite furnace and the rf electrode . Since the reflected power changes late into the atomization step, application of higher rf power becomes difficult. The rf power supply and matching network employed for this study were designed for semiconductor plasma processing work. Therefore, the reasonable remedy for the problem of variable rf power dissipation by the plasma would be to modify the matching

network to deliver a constant rf power during the high temperature ramp of the atomization step to prevent the extinguishing of the plasma. Furthermore, the electrical characteristics of this atmospheric pressure plasma source are not yet well understand. To understand the plasma extinguishing, a comprehensive study of the current-voltage characteristics of the plasma should be carried out.

A smaller plasma source workhead having reduced void volume than the present one would allow faster cooling of the graphite furnace and the furnace mount. Difficult and time consuming sample deposition on the inner wall of the furnace can also be avoided by using an auto sampler instead of manual injection. In addition, the use of a higher heating rates for the graphite furnace during the atomization step would be beneficial to improve the analytical characteristics.

This thesis presents a study of the effect of radio frequency power on the helium plasma source in FAPES as a spectrometric source for chemical analysis. This study provides an useful understanding of physical phenomenon occurring in the plasma at a fundamental level. This thesis also suggests further studies to improve the understanding and to modify the instrumentation to make the plasma stable at higher rf powers and higher furnace temperature.

BIBLIOGRAPHY

1. A. Walsh, *Spectrochim. Acta,* 108, **7** (1955).
2. B.V.L'vov, *Spectrochim. Acta,* 761, **17** (1961).
3. W. Slavin, *Anal. Chem.*, 589A **58** (1986).
4. W. Slavin, *Trends Anal. Chem.*, 194, **6** (1987).
5. S. Murayama, *Spectrochim. Acta,* 191, **25B** (1970).
6. J. P. Matousek, *Prog. Anal. Atom. Spectrosc.*, 247, **4** (1981).
7. W. Frech, E. Lundberg and A. Cedergren, *Can. J. Spectrosc.* 123, **30** (1985).
8. W. Trappe and J. Van Calker, *Z. Anal. Chem.* ,13 ,**198** (1963).
9. E. Badarau, M. Giurgea and A.T.H. Trutia, *Spectrochim. Acta,* 441, **11B** (1956).
10. R. H. Wendt and V. A. Fassel, *Anal. Chem*, 920, **94** (1965).
11. S. Greenfield, L. Jones and C. T. Berry, *Analyst* 713, **89** (1964).
12. H. Falk, C.R.C. Crit, *Rev. Anal. Chem.*,29, **19** (1988).
13. D. Littlejohn and J. M. Ottaway, *Analyst* 208, **104** (1079).
14. J. M. Ottaway and F. Shaw, *Analyst*,438,**100** (1975).
15. D. Littlejohn and J. M. Ottaway, *Analyst* , 553,**102** (1977).
16. H. Falk, E. Hoffmann, I. Jaeckel and Ch. Ludke, *Spectrochim. Acta* , 333, **34B** (1979).
17. H. Falk, E. Hoffmann, and Ch. Ludke, *Spectrochim. Acta* , 767, **36B** (1981).
18. H. Falk, E. Hoffmann, and Ch. Ludke, *Spectrochim. Acta* , 283, **39B** (1984).

19. N. E. Ballou, D. L. Styris and J. M. Harnly, *J. Anal. At. Spectrom.,* 1141, **3** (1988).

20. N. E. Ballou, D. L. Styris and J. M. Harnly, *J. Anal. At. Spectrom.,* 139, **5** (1990).

21. N. E. Ballou, D. L. Styris J. M. Harnly and P.G. Riby, *Spectrochim. Acta,* 203, **46B** (1991).

22. D.C. Liang and M.W. Blades, *Spectrochim. Acta*, 1059, **44B** (1989).

23. R. E. Sturgeon, S.N. Willie, V. Luong and S. S. Berman, *J. Anal. At. Spectrom.*, 669, **4** (1989).

24. D. L. Smith, D.C. Liang, D. Steel and M.W. Blades, *Spectrochim. Acta*, 493, **45B** (1990).

25. K. W. Jackson and H. Qiao, *Anal. Chem.*, 50R, **64** (1992).

26. B. V. L'vov, *Spectrochim. Acta,* 53, **24B** (1969).

27. B. V. L'vov, *Spectrochim. Acta,* 153, **33B** (1978).

28. W. Slavin and D. C. Manning, *Spectrochim. Acta,* 701,**35B** (1980).

29. W. Slavin and G. R. Carnric, , *Spectrochim. Acta,* 271,**39B** (1984).

30. R. E. Sturgeon and C. L. Chakrabarti, *Spectrochim. Acta,* 231, **32B** (1977).

31. J. E. Marshall, D. Littlejohn, J. M. Ottaway, J. M. Harnly, N. J. Miller-Ihli and T. C. O'Haver, *Analyst*, 178, **108** (1983).

32. W. Frech, D. C. Baxter and B. Hutsch, *Anal. Chem.*, 1973, **58**, (1986).

33. D. C. Duckworth and R. K. Marcus, *Anal. Chem.*, 1879, **61** (1989).

34. M. R. Winchester, C. Lazik and R. K. Marcus, *Spectrochim. Acta,* 438, **46B** (1991).

35. H. A. Schwab, *Proc. I. E. E. E.*, 613, **59** (1971).

36. H. A. Schwab and C. K. Manka, J. Appl. Phys., 696, 40 (1969)

37. H. A. Schwab and R. F. Hotz, *J. Appl. Phys.*, 1500, **41** (1970).

38. H. A. Schwab and R. F. Hotz, *J. Appl. Phys.*, 1503, **41** (1970).

39. H. Norstrom, *Vacuum*, 341, **29** (1979).

40. H. R. Koenig and L. I. Maissel, *IBM J. Res. Develop.*, 168, **14** (1970).

41. H. Y. Fan, Phy. Rev., 769, 55 (1979).

42. H. R. Griem, Plasma Spectroscopy, McGraw-Hill, New York, 1964.

43. P. W. J. M. Boumans, Theory of Spectrochemical Excitation, Hilger and Watts, London, 1966.

44. E. U. Condon and H. Odishaw in *Hand Book of Physics*, 2nd Edition, Published by McGraw-Hill Book Company, p.8-76--8-84, (1967).

45. T. D. Hettipathirana and M. W. Blades, *Spectrochimica Acta*, 493, **47B** (1992).

46. C. W. Collins and W. W. Robertson, *J. Chemical Physics*, 701, **40** (1964).

47. M. Endoh, M. Tsuji and Y. Nishimura, *J. Chemical Physics*, 5368, **79(11)** (1983).

48. R. E. Sturgeon, S. N. Willie, V. T. Luong and S. S. Berman, *Anal. Chem.*, 2370, **62** (1990).

49. R. E. Sturgeon, S. N. Willie, V. T. Luong and J. G. Dunn, *Appl. Spectrosc.,* 1413, **45** (1991).

50. R. E. Sturgeon, S. N. Willie and V. T. Luong ,*Spectrochiimica Acta,* 1021, **46B** (1991).

51. R. E. Sturgeon, S. S. Berman and S. Kashyap, *Anal. Chem.,* 1049, **52** (1980).

52. W. D. Westwood, *Prog. Surf. Sci.*, 71, **7** (1976).

53. H. Falk, E. Hoffman and C. Ludke, *Prog. Anal. Spectrosc.*, 417, **11**(1988).

54. L. de Galan, *Spectrochim. Acta.* , 537, **39B** (1984).

55. S. L. Paveri-Fontana, G. Tessari and G. Torsi, *Anal. Chem.* , 1032, **46** (!974).

56. G. Tessari and G. Torsi, *Anal. Chem.* , 839, **47** (1975).

57. D. A. Bass and J. A. Holcombe, Spectrochim. Acta, 1473, **43B** (1988).

58. S. J. Cathum, C. L. Chakrabarti and J. C. Hutton, Spectrochim. Acta, 35, **46B** (1991).

59. W. Slavin and D. C. Manning, *Spectrochim. Acta,* 955,**37B** (1982).

60. T. D. Hettipathirana and M. W. Blades, *Analytical Atomic Spectrometry,* 1039, **7**, (1992).

61. P. G. Riby, J. M. Harnly, D. L. Styris and N. E. Ballou, *Spectrochim. Acta,* 203, **46B** (1991).

62. A. Savitzky and M. J. E. Golay, *Anal. Chem.* 1627, **36** (1964).

63. B. V. L'vov, A. V. Novichikhin and L. K. Polzik, *Spectrochim. Acta,* 289, **47B** (1992).

64. P. Hocquellet, *Spectrochim. Acta*, 719, **47B** (1992).

65. W. L. Winterbottom and J. P. Hirth, The Vaporization Kinetics of Solid Silver, Ed. ; E. Rutner, P. Goldfinger and J. P. Hirth, Condensation and Evaporation of Solids ; Science Publishers, New York, 1964, P. 348.

66. J. M. Harnly, D. L. Styris and N. E. Ballou, *J. Anal. At. Spectrom.,* 139, **5** (1990).